SSRG International Journal of Civil Engineering
ISSN: 2348-8352/ https://doi.org/10.14445/23488352/IJCE-V13I11P103

Volume 13 Issue 11, 44-66, November 2026
© 2026 Seventh Sense Research Group®

Original Article

Aerodynamic Interference and Wind Pressure Effects in X-Shaped Tall Buildings under Variable Spacing Conditions

Mohammed Tosif Ahmed[1], Hemaraju Pollayi[2]

[1,2]*Department of Civil Engineering, GITAM Deemed to be University, Hyderabad, Telangana, India.*

[1]*Corresponding Author: mahmed6@gitam.in*

Received: 21 September 2026 Revised: 12 October 2026 Accepted: 20 October 2026 Published: 27 November 2026

Abstract - *With the increase of city populations, buildings' interactions under the viewpoint of aerodynamics have been more important, particularly for tall buildings whose plan shapes have become more complex and non-convex in nature. This computer study investigates the aerodynamic interference and wind-pressure characteristics among X-shaped tall structures, surrounded by octagonal, Y-shaped and rectangular buildings for different inter-building spacing variables. The conventional k-ε turbulence model is used to perform steady-state Reynolds-averaged Navier-Stokes simulations with a wind incidence angle of 0°. The mean pressure coefficients and interference factors are tested for different lateral and longitudinal spacings of the test models in the isolated and interference cases. Because of flow channeling, shielding and the interaction with the wake, the surface pressure is found to be strongly redistributed in space. The face-wise interference response is quite spacing and building-face-position dependent, with height-averaged interference factors around 1.11 for a windward face and 1.46 for a leeward face. For lateral separation, where these wakes could still give rise to local reamplification as a result of wake contact and flow reattachment, the overall response is not monotonic with lateral separation distance. The overall value for the interference response decreases with an increase in the longitudinal distance S_2; however, for $S_2 = 1B$, a considerable shielding for $S_1 = S_3 = 10B$ can be sensed. The findings indicated that the spacing along the building face, besides spacing forth and back, are the determinants of interfering. For tall buildings having complex plans, it is important to consider the geometry, spacing between other neighbouring buildings and their affected wind face when assessing the stresses the wind places on them. Further research and study is recommended on aeroelastic effects, wind from various angles.*

Keywords - *Computational Fluid Dynamics, High-Rise structures, Pressure coefficient, Wind interference, X-Shaped building.*

1. Introduction

With the arrival of rapid urbanization and the vertical development of cities, high-rise buildings have been gradually concentrated in the high-density urban environment. Pressure distribution, wind speed and wind direction around a single building are affected by the wind field, which is changed by the neighbouring buildings. Depending on the relative position and geometry of the buildings, these interactions can yield shielding, channelling, wake interference and pressure amplification. While adjacent buildings are typically considered to offer wind protection, interference effects can be one source of wind-induced pressures and structures' responses for certain building configurations [1]. Additionally, the urban canopy characteristics are also affected by the variations of the building heights, which affect the wind flow in the built-up areas [2].

In recent years, non-conventional building geometries have become an increasingly integral part of architectural design to realize functional, aesthetic and performance-related purposes. But it can be seen that changes in building geometry can have significant impacts on the aerodynamic characteristics of tall structures.

Das et al. studied the aerodynamic shape optimization of the corner-recessed square tall buildings by surrogate modelling [3] while Kumar and Dalui focused on the effect of the internal angles between the limbs of the tall buildings for cross-plan shape under wind loading [4]. Thepmongkorn et al. showed the influence of relative positioning of buildings on interference-induced coupled motion of tall buildings [5]. Tang and Kwok also studied the interference excitation between two tall buildings, and emphasized the importance of building interactions on wind-induced structural responses [6]. Interference between twin C-shaped tall buildings was then investigated by Verma and Sonparote, showing the relevance of complex geometries of the plans in interference-related investigations [7].

This is an open access article under the CC BY-NC-ND license (http://creativecommons.org/licenses/by-nc-nd/4.0/)

Experimental and numerical studies have also shown that building geometry and spatial location affect pressure distributions and aerodynamic forces due to wind. Nagar et al. conducted experiments to study pressures on tall buildings of different plan shapes when subjected to wind [8], and Zhao and Lam studied interference effects between groups of tall buildings arranged in L- and T-shaped form [9]. Agarwal et al. [10] studied the effect of interference of wind pressure for rectangular plan tall buildings.

In a similar investigation, Tanaka et al. investigated the effects of aerodynamic forces and pressures on tall buildings that have both helical and corner modified structures, and demonstrate that the geometry of the structure may affect the aerodynamic behavior of tall building [11]. All of these studies confirm the significance of building shape, relative positioning and surrounding configuration to study the wind-induced effects on tall buildings.

Wind-resistant design is generally guided by established standards, including ASCE/SEI 7-10 [12], IS 875 (Part 3):2015 [13], and AS/NZS 1170.2 [14]. These standards offer guidance on how to assess wind forces on buildings and structures. However, considering interference effects that may not be accurately described by the assessment of a single building must be included when predicting the aerodynamic behavior of complex building arrangements. Khanduri et al. [15] have given a thorough discussion about the wind-induced interference effects on buildings and highlighted the importance of the surrounding buildings in wind engineering. Computational Fluid Dynamics (CFD) is an important computational tool used to understand the wind flow, pressures and aerodynamic interactions of a high-rise building and complex urban areas in this context [16].

More work has been focused on the aerodynamic aspects of buildings of other plan configurations. Sanyal and Dalui studied the aerodynamic coefficient of Y-shaped tall buildings [17]. The dimensional variations have also been studied in terms of wind-pressure distributions, revealing that the geometric parameters can affect the spatial aspects of wind-induced loading [18]. Reynolds-Averaged Navier–Stokes (RANS) equations are a well-established approach for turbulence modelling in numerical investigation of turbulent wind flow [19]. Numerical tools have been used to study wind distributions around buildings in low-density urban areas through CFD modelling, which demonstrates their usefulness in the analysis of the building-scale flow patterns [20]. For reliable CFD-based wind engineering investigations, however, the configuration of the computational domain, the boundary conditions, turbulence modelling, and the procedures used to validate the model are all important [21]. In particular, numerical simulations of wind flow around buildings are important for the representation of the atmospheric boundary layer and treatment of wall functions [22].

Research on other non-conventional geometries has also helped to develop knowledge of building aerodynamics. Plan geometry was also found to be relevant for the aerodynamic assessment, as demonstrated by Paul and Dalui's analysis of wind effects on Z-plan-shaped tall buildings [23]. For a bluff in the turbulent boundary layer, fundamental studies of the forces acting on the bluff are important in understanding flow separation and pressure distributions around buildings [24]. Kim et al. studied interference effects on aerodynamic forces between two buildings [25], and Nakayama et al. studied turbulent flow over building arrays with Large-Eddy Simulation (LES) [26]. The wake interactions of two square cylinders side by side have also been studied that can help understand flow interactions between neighbouring bluff bodies [27]. Moreover, Kar and Dalui studied the wind interference on an octagonal-plan tall building, due to the surrounding square-plan tall buildings [28]. Ishida et al. studied the effects of a single high-rise on adjacent low-rise buildings, which is the discussion of building interference to different height buildings [29]. Bharat Singh Chauhan et al. also studied the wind-load properties of tall buildings of rectangular plan under interference conditions [30].

The use of CFD in wind engineering has been reported in recent technical reviews recently, where tall buildings and structure assessment and design have been reviewed [31]. Results from numerical investigations of Y-shaped tall buildings with wind loads, which were investigated using CFD, are also presented in the context of other unconventional building shapes [32]. Further studies have investigated the types of interference excitation mechanisms through the use of aeroelastic building models to gain an understanding of the relationship between the surrounding-building configurations and the responses of the building to wind loads [33]. Another important reference configuration for wind-tunnel measurements under simulated atmospheric boundary-layer conditions has been the CAARC (standard tall building model) [34]. Although these developments have taken place, the simultaneous effects of complicated principal building geometry, neighbouring building shape, and varying inter-building distances are still significant parameters that warrant further investigation.

Most of the previous studies have focused on the traditional plan configurations, chosen the non-traditional plan shapes or considered relatively simple forms of interference configurations. Studies on cross-shaped, C-shaped, Y-shaped, Z-shaped, rectangular, and octagonal buildings have helped to understand the pressures applied by wind on a building and the aerodynamic interference between multiple neighbouring buildings of various plan shapes, but systematic investigations with an X-shaped principal building surrounded by a number of neighbouring buildings of various plan shapes are still limited. Specifically, the response of the face-wise pressure of a complex non-convex principal building to neighbouring building geometry and longitudinal and lateral distances has

yet to be quantified as a combined effect. Spatial variation of interference on individual faces, including pressure amplification, shielding, channelling and wake interactions, thus need to be examined further.

To fill this research gap, a study based on Computational Fluid Dynamic (CFD) simulation of an X-shaped tall building surrounded by rectangular-, octagonal-, and Y-shaped neighbouring buildings under various spacing conditions is conducted. The aerodynamic response is assessed under isolated and interference conditions with respect to the face-wise pressure coefficients and interference factors. Special focus is placed on the effect of the geometry of adjacent buildings and on the interference distribution between longitudinal and lateral spacing between buildings on the principal building's faces. Therefore, the aim of this study is to: (i) Calculate the face-wise pressure response and interference factors of the building having X-shape under isolated and interference conditions. (ii) Investigate how the geometry of the surrounding buildings and longitudinal and lateral distances between the buildings influence the spatial distribution of aerodynamic interference effects. (iii) Under various neighbouring building configurations, determine the characteristics of flow interaction related to pressure amplification, shielding, channelling and wake interaction.

1.1. Physical Model and Baseline Configuration

1.1.1. Geometry of the Principal X-Shaped Building

The present research mainly focuses on a typical tall building that forms an X shape with a full-scale height of 180 m, width of 30 m and length of 45 m. The geometric scale of the model used in the CFD simulation is 1:300, with a length, a width and a depth of, respectively, 600 mm, 100 mm and 150 mm. This scale is consistent with established wind engineering practice and ensures adequate resolution of flow features while maintaining a manageable computational cost. As the present study focuses on non-dimensional pressure coefficients and interference factors, the Reynolds number independence was assumed for the high-Reynolds-number flow regime considered [24]. Previous experimental and numerical studies on sharp-edged bluff bodies have demonstrated that the mean pressure coefficients become Reynolds number independent above $Re \approx 1 \times 10^5$, justifying the present assumption for high-Reynolds-number atmospheric flow conditions. Its dimensions and planar geometry is shown as in Figure 1. The geometry of all plan variations stayed within a plan envelope of 45 m × 30 m with the aim of ensuring geometric comparability between various plan configurations. These variations are in the form of rectangle, octagon, Y, X. The rectangular design corresponds to the standard building model for CAARC, for which it was the spawning ground in the first place. In the X-shaped design, four symmetrical wings are radiating from the center of the design. This wings present many re-entrant corners and different sharp edges that have a considerable effect on the flow separation and the development of the vortices. To measure the pressure around the exterior of the building, the walls of the building were divided into 16 faces labeled, clockwise, from A to P. A systematic comparison of the pressure distribution was then made on the side, windward, and leeward sides from face to face, as shown in Figure 1.

For the scaled principal building, the height is H=600 mm, and the characteristic breadth is B=150 mm, giving B/H=0.25. Therefore, the relationship between the B-based spacing and the nondimensional spacing ratio is S/H=0.25(S/B). This gives S/H=0.50, 1.25, 2.00, and 2.50 for longitudinal spacings of 2B, 5B, 8B, and 10B, respectively. For the lateral spacings of 1B, 3B, 5B, and 8B, the corresponding values are S/H=0.25, 0.75, 1.25, and 2.00, respectively.

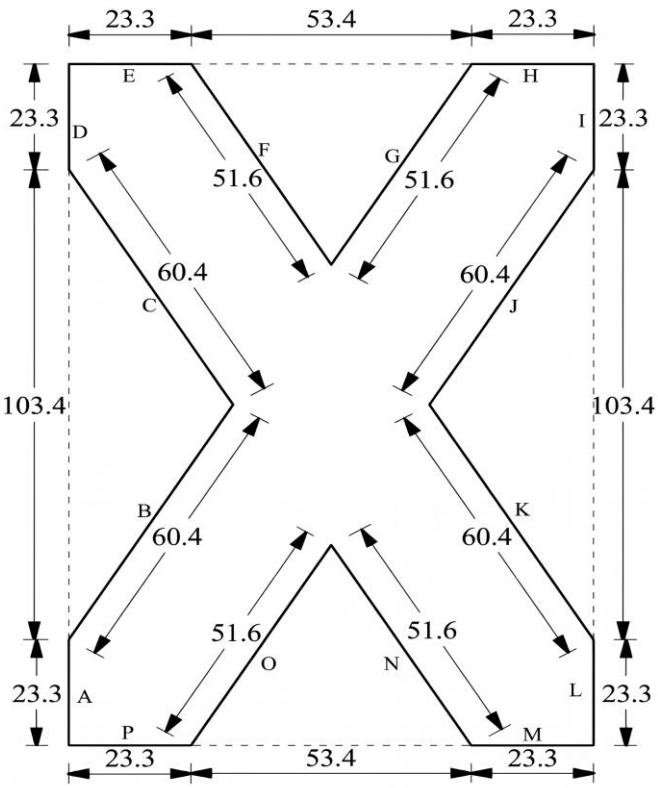

Fig. 1 X-shaped building dimensions

1.1.2. Baseline Isolated Configuration

The baseline case is an isolated configuration where there are no surrounding buildings, which is an undisturbed flow of the atmospheric boundary layer hitting the main building. This case is used to assess interference effects and to calculate the Interference Factors (IFs), which are defined as the pressure coefficient in interference conditions divided by that in isolated conditions. This base condition enables that all pressures that have been altered by the interference to be measured against a standard, which helps to separate the variations caused by adjacent geometry and spacing from the aerodynamic characteristics of the X-shaped planform.

1.1.3. Surrounding Building Shapes and Layout

Three surrounding building plan shapes (rectangular, octagonal and Y-shaped) were chosen as representative plan shapes of contemporary urban buildings and their wakes. To examine the effects of planform geometry and spacing on aerodynamic interference, all surrounding buildings were modelled to match the height of the principal X-shaped building and to have similar plan dimensions. This assumption removes height-related shielding or amplification effects, allowing for a more in-depth analysis of interference behavior in a plan. The interference configuration shown in Figure 2 was investigated at a wind incidence angle of 0°. The longitudinal spacing between the upstream octagonal building and the principal X-shaped building, denoted by S_1(Horizontal distance), was varied along with the longitudinal spacing between the principal X-shaped building and the downstream rectangular building, denoted by S_3(Vertical distance). The lateral spacing between the octagonal and Y-shaped buildings, denoted by S_2, was also varied. For each configuration, the longitudinal spacings were maintained equal ($S_1 = S_3$), while S_2 was varied independently. To limit the number of parameters, the upstream and downstream spacings were fixed for each configuration, with the primary role being to control the wake recovery. Four spacing cases were analysed: Case 1 ($S_1 = S_3 = 2B$), Case 2 (5B), Case 3 (8B), and Case 4 (10B), with lateral spacings (S_2) of 1B, 3B, 5B, and 8B. Based on the nondimensional interpretation, the typical width of the major building model (B=150 mm) and the typical height of the major building model (H=600 mm) has a ratio of 0.25. Consequently, S/H=0.25(S/B). At 2B, 5B, 8B, and 10B along the longitudinal axis, S/H=0.50, 1.25, 2.00, and 2.50 correspondingly, while at 1B, 3B, 5B, and 8B along the lateral axis, S/H=0.25, 0.75, 1.25, and 2.00 correspondingly. In order to give a uniform description of the configurations analyzed, both physical spacing (b) and nondimensional S/H are reported. Table 1 shows that the building-spacing configurations studied have been summarized below.

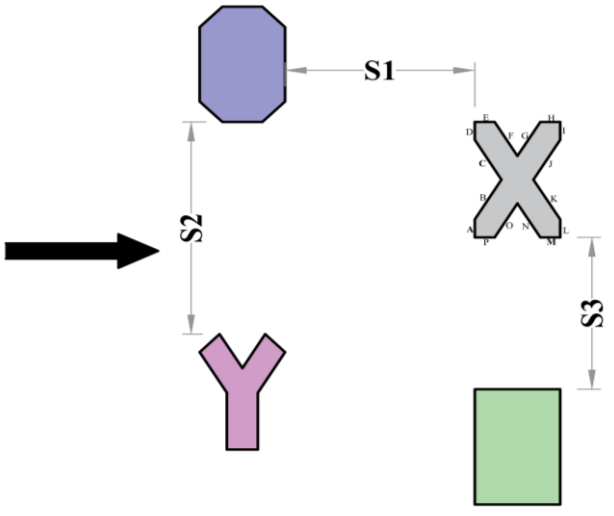

Fig. 2 Plan view of principal and interference buildings

Table 1. Arrangement of building spacing cases for interference study

Case	S1 (Upstream)	S2 (Lateral – Varied)	S3 (Downstream)
Case 1	2B (300 mm)	1B (150 mm)	2B (300 mm)
		3B (450 mm)	
		5B (750 mm)	
		8B (1200 mm)	
Case 2	5B (750 mm)	1B (150 mm)	5B (750 mm)
		3B (450 mm)	
		5B (750 mm)	
		8B (1200 mm)	
Case 3	8B (1200 mm)	1B (150 mm)	8B (1200 mm)
		3B (450 mm)	
		5B (750 mm)	
		8B (1200 mm)	
Case 4	10B (1500 mm)	1B (150 mm)	10B (1500 mm)
		3B (450 mm)	
		5B (750 mm)	
		8B (1200 mm)	

Note: B = 150 mm is the characteristic breadth of the principal building model (corresponding to 45 m in full scale).

2. Computational Methodology

2.1. Governing Equations

The incompressible Reynolds–Averaged Navier–Stokes (RANS) equations and the standard k–ε turbulence model [19] were employed for the simulations of the aerodynamic processes around the tall X-shaped building. This technique is often employed in wind engineering for high Reynolds number flows in the atmospheric boundary layer, where it is a compromise between the computational efficiency and the prediction of mean surface pressure [20]. The steady state RANS model was used to determine time-averaged flow parameters and facade pressure coefficients for along-wind load and interference studies. Vortex shedding and unsteady wake dynamics were not investigated in the present steady-state simulations and are left for future research. The equations were solved under steady state conditions with second-order upwind discretization of momentum and turbulence terms with the model constants of Launder and Spalding (1974). Convergence was found when the scaled continuity and momentum residuals became less than a certain threshold.

2.2. Computational Domain

The computational domain was set up according to the guidelines of Franke et al. (2004) for wind engineering CFD [21, 22]. The domain configuration and boundary assignments are shown in Figure 3. To reduce blockage and allow for a full development of the wake, the domain is extended 5H upstream, 15H downstream and 5H laterally and vertically,

with H being the building height [21]. The ratio of blockage is less than 3%, which is the recommended ratio.

A full-scale reference wind velocity of U_{ref}=50 m/s was considered, while an inlet reference velocity of 10 m/s was adopted for the scaled CFD model (1:5). The inlet was prescribed using a power-law atmospheric boundary-layer profile for terrain category II (α=0.133), with the reference velocity specified at z_{ref}=1.0 m [23].

$$U(z) = U_{ref}\left(\frac{z}{z_{ref}}\right)^{\alpha}$$

The power law exponent is α=0.133 with Uref=10 m/s as the reference wind velocity, zref=1.0 m as the reference height, and U(z) as the mean wind velocity at height z, terrain category II. The exit was a pressure outlet (p=0 Pa), and turbulent viscosity ratio = 10, while the initial turbulent intensity of the inlet was 5%.

The whole structure and the ground below was covered with the static (non-slip) walls. Treatment used for near-wall regions was enhanced wall treatment; wall y+ values varied from 0.875 to 4.793, and ranged most of the way from 1.445 to 2.016 on an area-weighted basis [22]. The Reynolds number was determined, using a model height of 0.60 m and the reference air speed of 4.11 x 105.

Due to the symmetry planes, the top and sides of the computing domain were defined. The pressure-approach to steady-state solving, pressure-equation and pressure-velocity equations and second-order discretization methods were employed on the simulation.

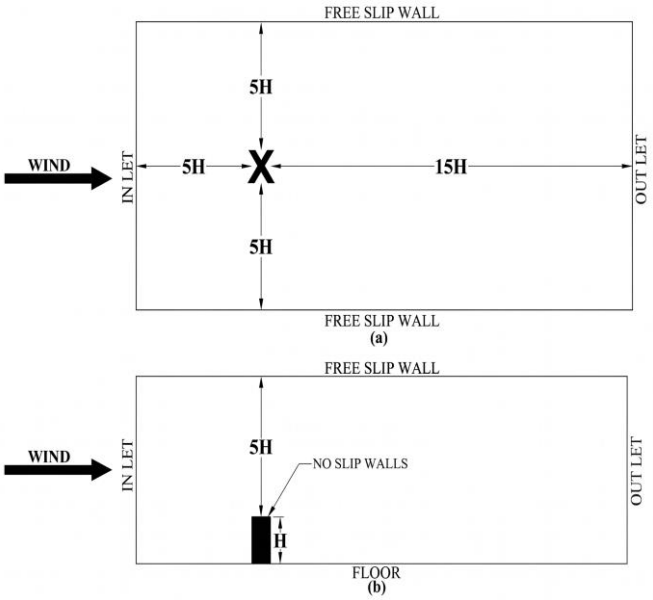

(a)

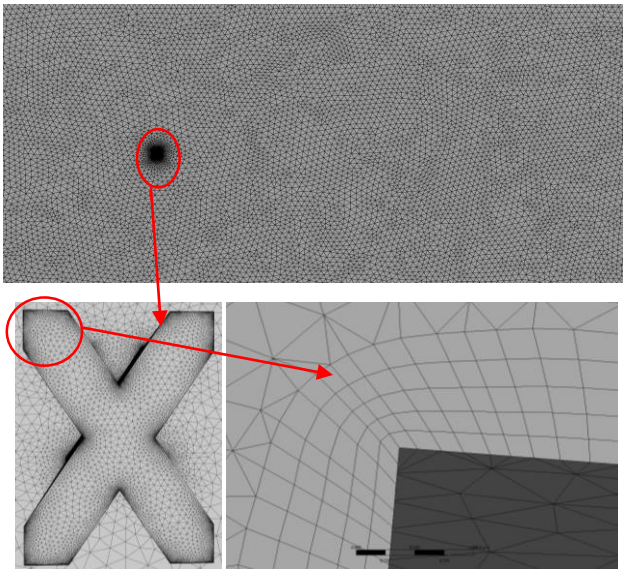

(b)

Fig. 3 Computational domain and mesh details: (a) Computational domain and boundary conditions, and (b) Computational mesh with local refinement around the X-shaped building.

2.3. Grid Independence and Numerical Stability Assessment

A grid independence study was performed using four mesh resolutions Coarse, Medium, Fine, and Very Fine to assess numerical stability and minimize discretization effects, as shown in Figure 4. The mean pressure coefficient at Face A was compared for the different mesh densities. As shown in Table 2, the mesh size increased from 2.1 × 10^6 to 12.3 × 10^6 elements, while the corresponding mean Cp values were 0.400, 0.386, 0.394, and 0.391, respectively.

The relative errors were calculated using the Very Fine mesh value as the reference and were 2.30%, 1.28%, and 0.77% for the Coarse, Medium, and Fine meshes, respectively. The relative difference between the Fine and Very Fine meshes was approximately 0.77%, indicating that further mesh refinement produced only a minor change in the calculated pressure coefficient. Therefore, the Fine mesh with 6.8 × 10^6 elements was selected for the subsequent simulations as a suitable balance between numerical accuracy and computational cost. Grid Independence study for x shape building in Isolated condition shown in Table 2.

Table 2. Grid independence study for x shape building in isolated condition

Mesh Level	Elements (×10^6)	Mean Cp at Face A	Relative Error (%)
Coarse	2.1	0.400	2.30
Medium	4.2	0.386	1.28
Fine	6.8	0.394	0.77
Very Fine	12.3	0.391	-

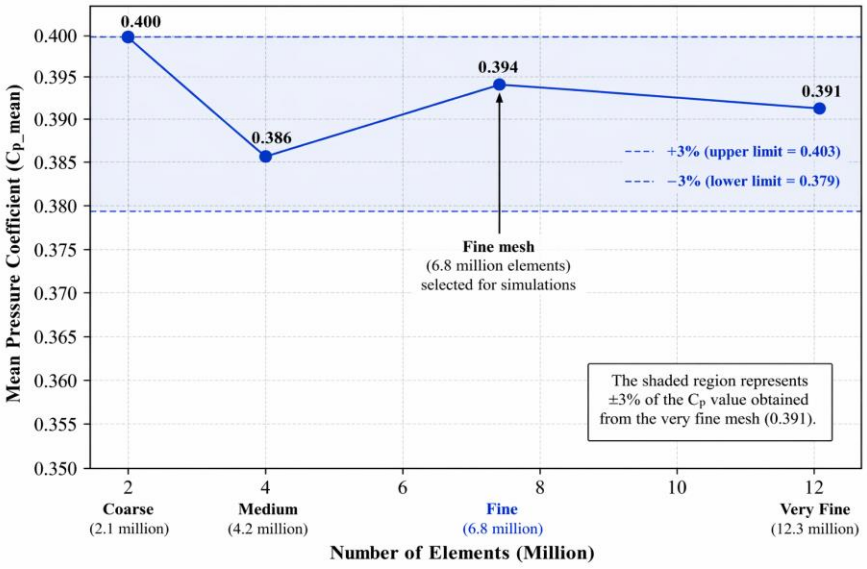

Fig. 4 Grid independence study showing the selection of the fine mesh (6.8 million elements)

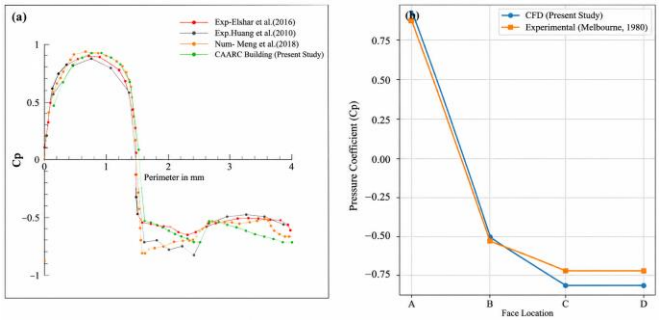

Fig. 5 The CAARC standard tall building [34] can be used to validate the numerical model in two ways: a comparison of the distributions of the perimeter pressure coefficient Cp with published experimental and numerical results, and a comparison of the present CFD results with the experimental data (Melbourne, 1980).

2.4. Validation

The numerical framework was validated using simulations of the CAARC standard tall building under the same atmospheric boundary-layer conditions, with the predicted perimeter and mean pressure coefficients compared with published wind-tunnel data. Compare results of the current Computational Fluid Dynamics (CFD) results to experimental data shown in Figure 5. No big variance on the windward side, however, little variations on the side and leeward sides. This may be related to the restrictions of turbulence modeling and/or the steady-state assumptions. The statistical match results in an R2 of 0.944 and an RMSE of ~ 0.054, with the total variation remaining within the limits of 15% either side. These results demonstrate satisfactory agreement between the CFD predictions and the experimental measurements for the perimeter and mean pressure distributions [34].

As an additional comparison, the Cp values obtained from the CAARC CFD simulation are compared with the corresponding values from IS 875, ASCE 7-10, and AS/NZS 1170.2 in Table 3. This comparison is intended to examine the consistency of the CFD-derived pressure coefficients with commonly used code-based values and is not considered as the experimental validation of the numerical model. For windward Face A, the CFD-derived pressure coefficient was 0.91, compared with 0.80 in both ASCE and AS/NZS and 0.95 in IS 875. The CFD value is 13.75% higher than the ASCE and AS/NZS values when the code value is used as the reference, whereas it is close to the IS 875 value. Larger differences are observed on the side and leeward faces (B–D), particularly for suction-dominated surfaces, where the IS 875 values show stronger suction than the CFD results and the other code-based values. These differences illustrate the variation between CFD-derived pressure distributions and simplified code-based pressure coefficients [12-14].

Table 3. Comparison of CFD-derived Cp values with code-based values

Face	CFD Cp	ASCE 7-10	AS/NZS	IS 875
A	0.91	0.80	0.80	0.95
B	-0.52	-0.30	-0.20	-1.85
C	-0.86	-0.70	-0.65	-0.90
D	-0.86	-0.70	-0.65	-0.90

3. Results and Discussion

This section explains the pressure distribution acting on the façade of the tall X-shaped building, as well as the aerodynamics of the flow in both isolated and interfering cases. We review the principal flow processes, neighboring structure pressure redistribution and building spacing to planform geometry.

3.1. Flow Characteristics under Isolated Condition

The flow around the X-shaped features was indicative of those that form sharp-edged bluffs in solitary flow. This air speeded up as it moved towards the windward faces (A–D), resulting in a well-defined stagnation region with an increase in positive pressure. Separation was noticed at the leading edges, and the shear layers stretched along the sides of the building and re-entrant surfaces (E–H and M–P). Proximity to these recessed areas allowed development of steady recirculation regions due to interaction between the separated flow and the complex plan geometry. The formation of the mean wake was observed downstream from the building, and was found to be of about 3.5-4H as was observed by others for non-convex polygonal structures. Figure 6 shows Flow pattern around isolated X-shaped building.

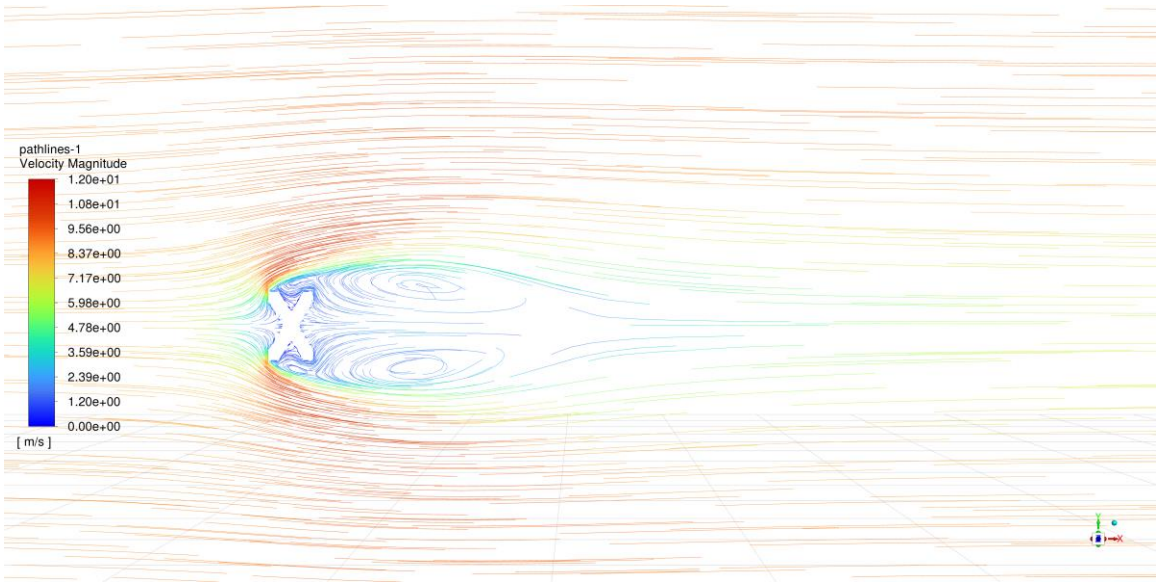

Fig. 6 Flow pattern around an isolated X-shaped building

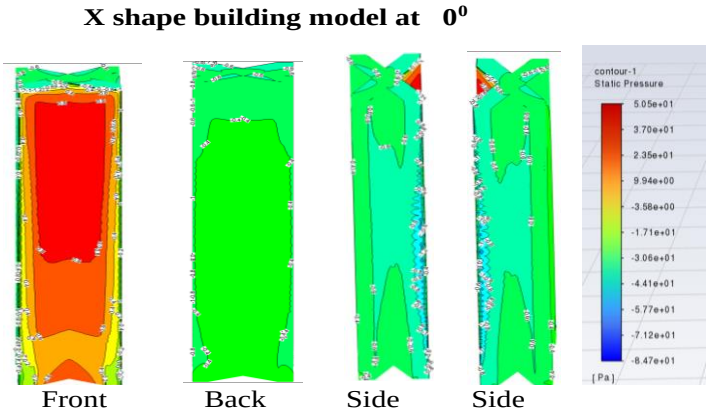

Fig. 7 Static pressure distributions on the four faces (front, back, and two side faces) of the isolated X-shaped building at a wind incidence angle of 0°, the colour legend indicates the static pressure on the building surfaces, expressed in Pa.

3.2. Pressure Contours on Each Side of the Building

The static pressure distribution around the X-shaped building model at 0° wind incidence [20] indicates the aerodynamic response of the bluffs with sharp edges. The stagnation zone causes the flow to slow down when it comes in contact with a high-pressure region in red (≈ +50 Pa) on the front (windward) side. The pressure deficit (≈ − 80 Pa) on the leeward face (back) is larger, leading to flow separation and a low-pressure recirculation area. The pressure gradients are moderate on the side faces, with the appearance of shear-layer

separation, deflection of the flow to the side, and gradually decreasing pressure from positive to negative. This distribution shows that the pressure drag is highest in the front to rear surfaces. Overall, as observed in the streamline pattern, the X-shaped geometry produces asymmetric pressure zones and high suction regions in its recesses, which is evidence for significant aerodynamic loading due to the wake in the 0° orientation [24, 25] (see Figure 7).

3.3. Pressure Coefficients for Isolated Condition

When the wind is unblocked, the building's windward faces are shown in Figure 7. Pressure values on the windward faces throughout the building height. The pressure is highest around the middle (where the wind is held), and is lowest near the roof (where the wind flows more freely). This pattern can be seen on the windward faces labeled A-D. The side and re-entrant faces (E to L) are under pressure in the building height because of the separation of the airflow at the edges, producing strong and fast-moving air layers. These faces are suctional in the centre and have systematically swirled air. As a result, the suction decreases at the bottom and top due to interference from the ground and the roof. There is strong suction on the leeward faces because of the air pressure behind the building, and a uniform suction distribution means that air circulates around the building nicely. The X-shape building illustrates the differences in air pressures on windward and leeward sides, illustrating how such buildings are influenced by air movement, particularly with swirls caused by the separation of air [16]. The pressure asymmetry suggests that the X-shaped plan is an aerodynamically weak design that can become more strongly aerodynamically loaded under interference flow conditions due to the presence of localised suction peaks.

3.4. Flow Characteristics under Interference Conditions

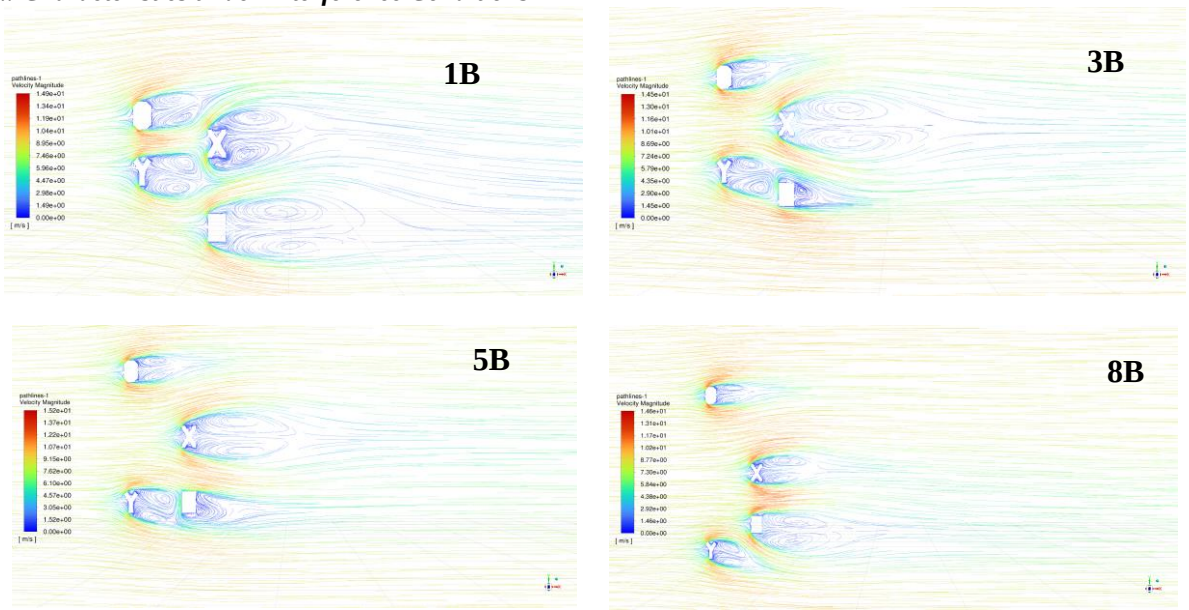

Fig. 8 Flow pattern around X shape building surrounded by different shapes buildings for Case I

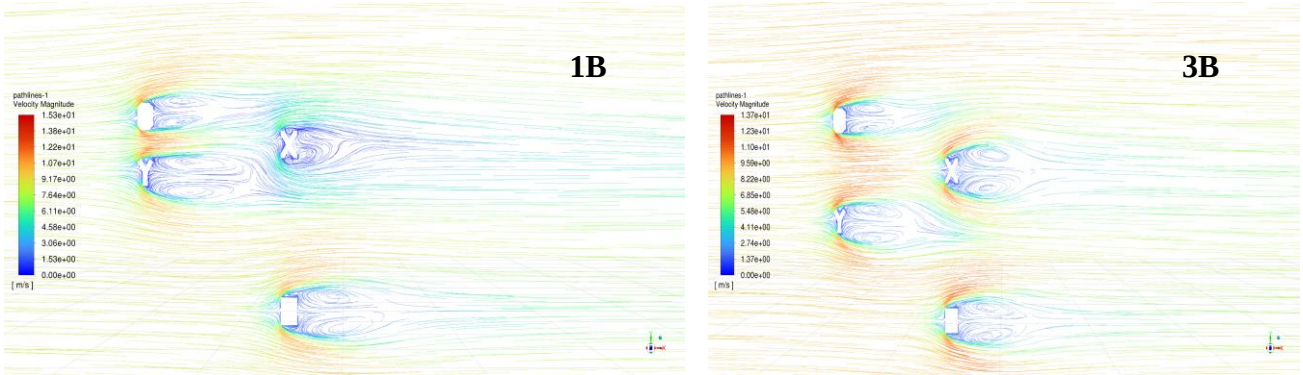

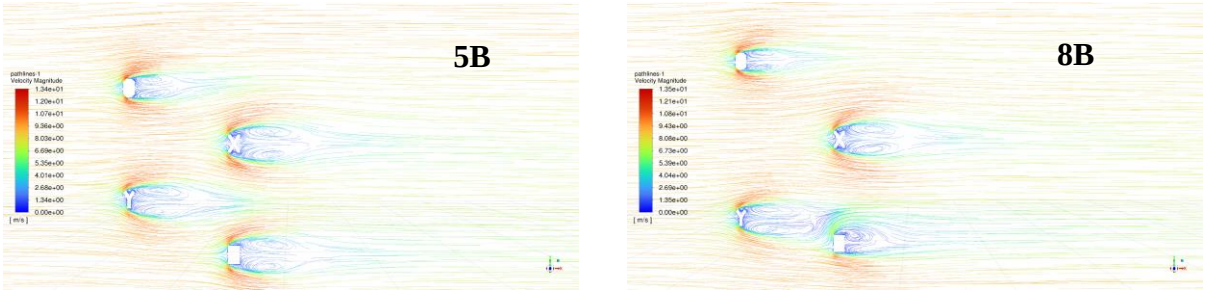

Fig. 9 Flow pattern around X shape building surrounded by different shapes buildings for Case II

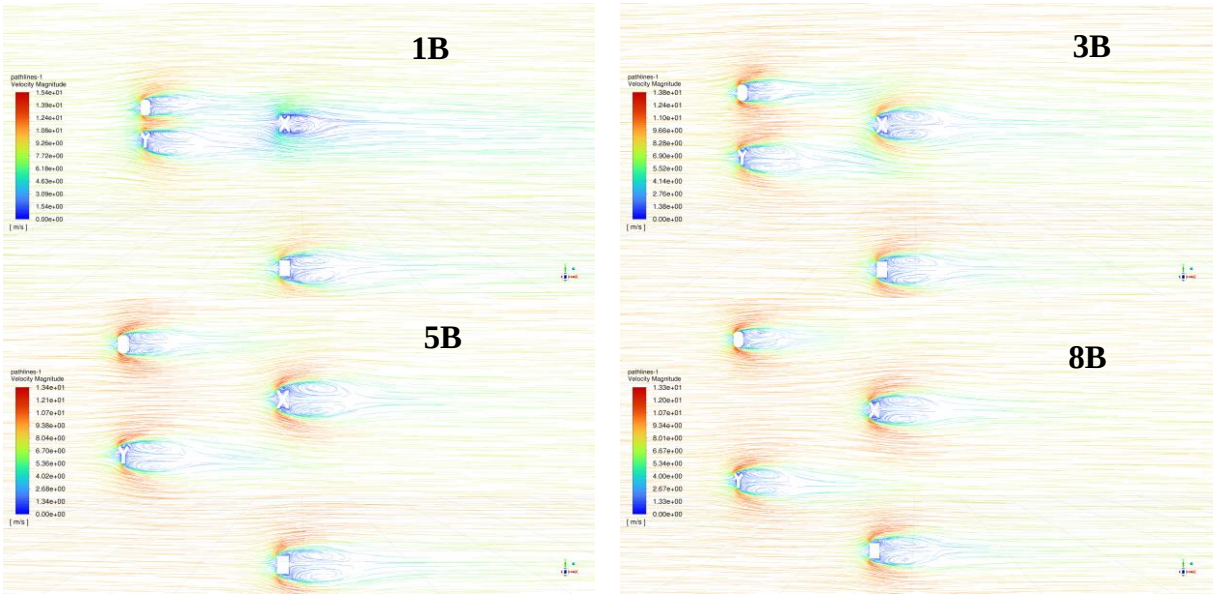

Fig. 10 Flow pattern around X shape building surrounded by different shapes buildings for Case III

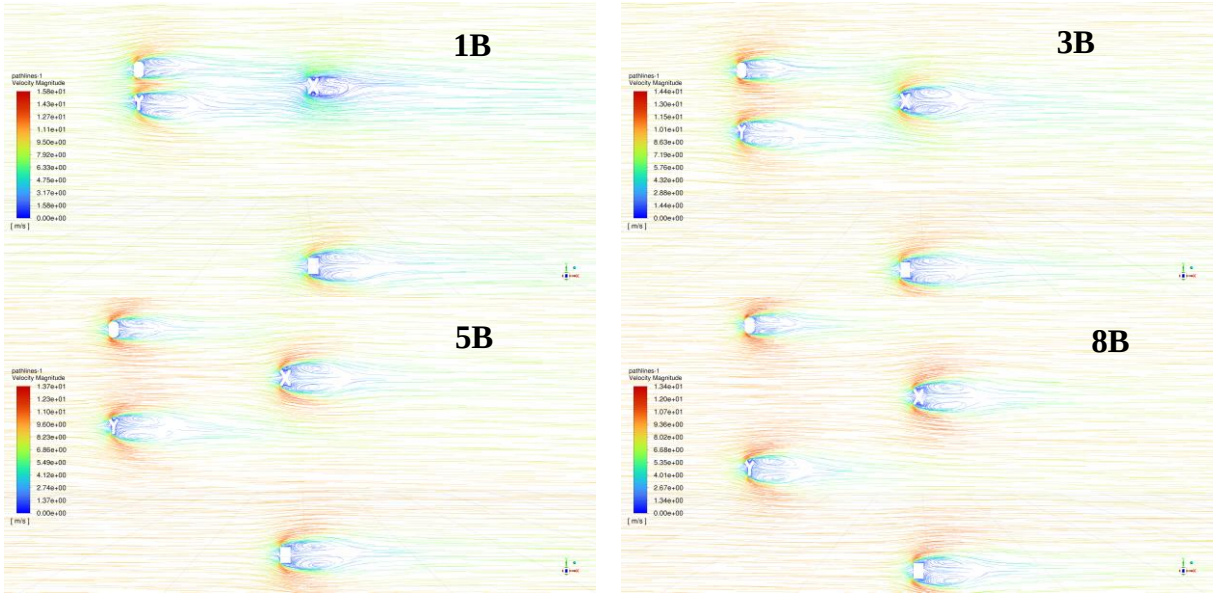

Fig. 11 Flow pattern around X shape building surrounded by different-shaped buildings for Case IV

For Cases I–IV, as the building spacing increases, the airflow around the buildings changes from turbulent to smooth. The airflow was greatly influenced by closely grouped octagonal and Y-shaped buildings upstream of the X-shaped building block, as seen in Case 1. This generated fast and slow air zones, strong jets attacking the X-shaped building, which led to flow separation and to a wake of 4.5 to 5.0 building widths downstream. There was strong vortex formation, and the downstream rectangular building had an impact on the wake growth and reattachment points. Moderate building spacing resulted in reduced wake effects because the air was partially recovered before reaching the building. The building has an octagonal shape to give wake protection, and a Y-shaped building to deflect the airflow [27]. The width of the wake is 2.5-3.0 times the building's width, and the velocity gradient layer is 30-40% thinner. The larger spacing allowed increased flow of air, resulting in an organised wake of 1.8–2.0 times the building width. Minimal effect from surrounding buildings since flow is almost symmetrical. For Case IV, where wake effects from adjacent buildings are not present to the main building, the flow patterns are symmetrical with a scale of 1.5-1.8 times the building width. The observed flow patterns indicate that interference is strongly influenced by building spacing and surrounding-building geometry [26]. The wake confinement is more severe for rectangular structures, the flow deflection is more uniform for octagonal buildings, and for buildings shaped like Y, the flow asymmetry is more concentrated at close spacings. These together affect the surface pressure pattern, which will be detailed later, and determining the spatial pattern and size of flow deviations produced by interference. Four cases were studied for the flow characteristics around the X-shaped building under the interference condition, taking into account the effect of surrounding buildings with different shapes. The flow patterns of cases I, II, III, and IV are shown in Figures 8-11, respectively. These figures show the differences in flow behaviour caused by the presence of and the layout of neighbouring buildings around the principal building. Moreover, the interference factors at various spacings, such as the 2b–1b, 2b–3b, 2b–5b and 2b–8b configurations on the face A–P are shown in the Figures 12-15, respectively. These contours help to determine interference effects caused by changes in the distance between the main building and other buildings.

3.5. Interference Factor Contour

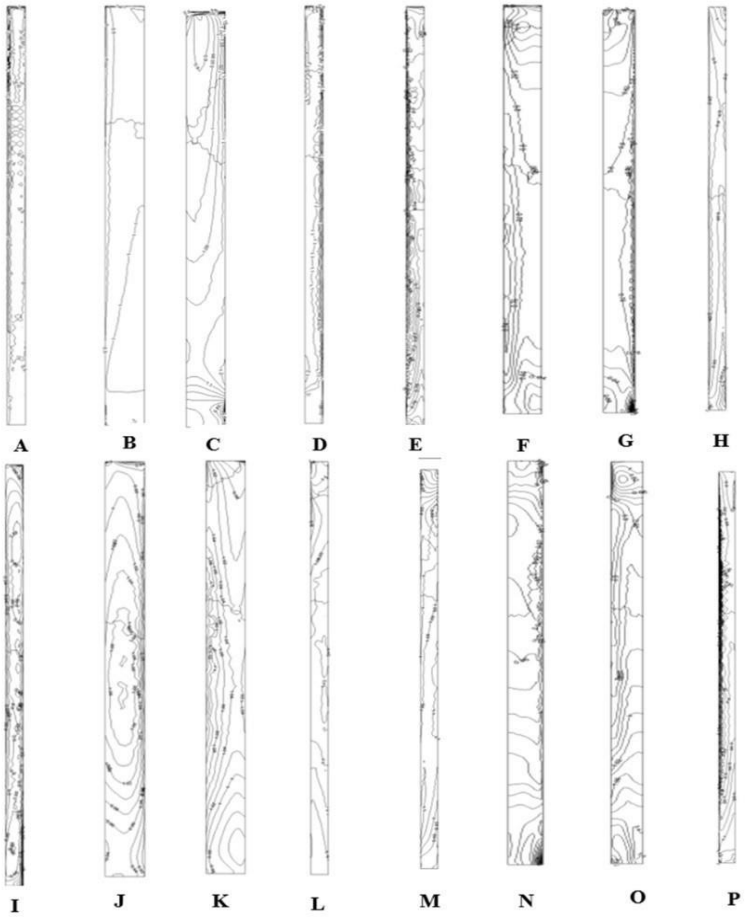

Fig. 12 Contours of interference factors [Case 1, 2b-1b] for a face A-P

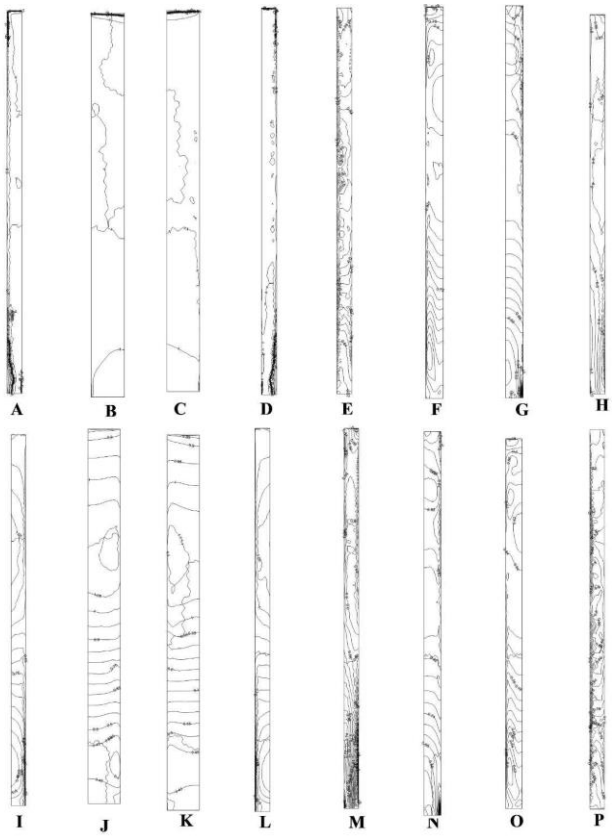

Fig. 13 Contours of interferencefactors [Case 1, 2b-3b] for a face A-P

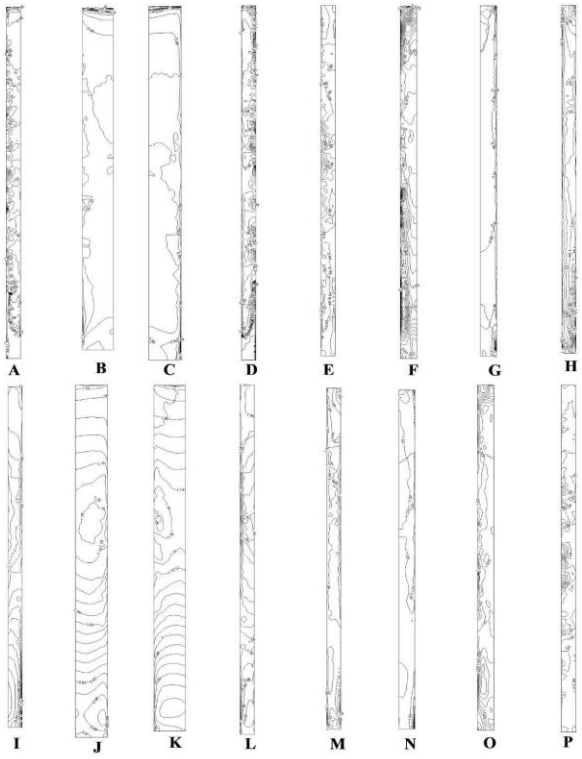

Fig. 14 Contours of interference factors [Case 1, 2b-5b] for a face A-P

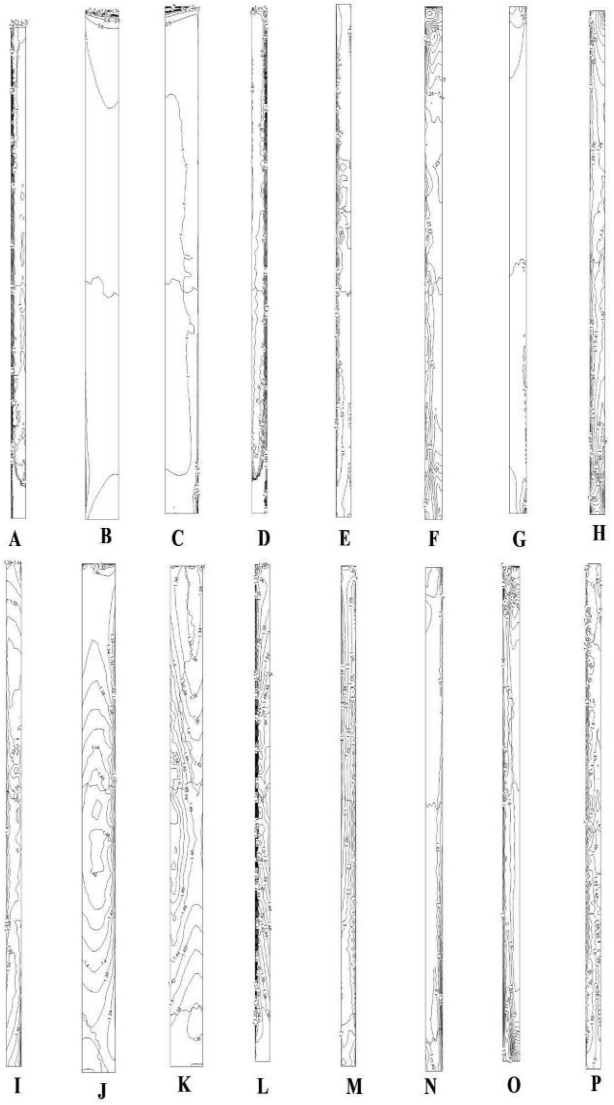

Fig. 15 Contours of interference factors [Case 1, 2b-8b] for a face A-P

Detailed Interference-Factor (IF) contour analysis is presented only for Case 1, corresponding to the selected critical interference configuration with the closest upstream and downstream spacing. This case is considered to examine the principal aerodynamic mechanisms associated with wake interaction, flow channelling and pressure redistribution around the X-shaped building.

Cases 2–4 are not presented as separate IF contour plots to avoid repetitive graphical presentation. However, the effects of spacing and surrounding-building geometry across all investigated cases are evaluated using the face-wise mean pressure coefficients and numerical IF results presented in the subsequent sections. This approach helps identify the principal interference mechanisms and supports a geometry- and spacing-dependent assessment of aerodynamic interference.

3.6. Cp Variation along Height

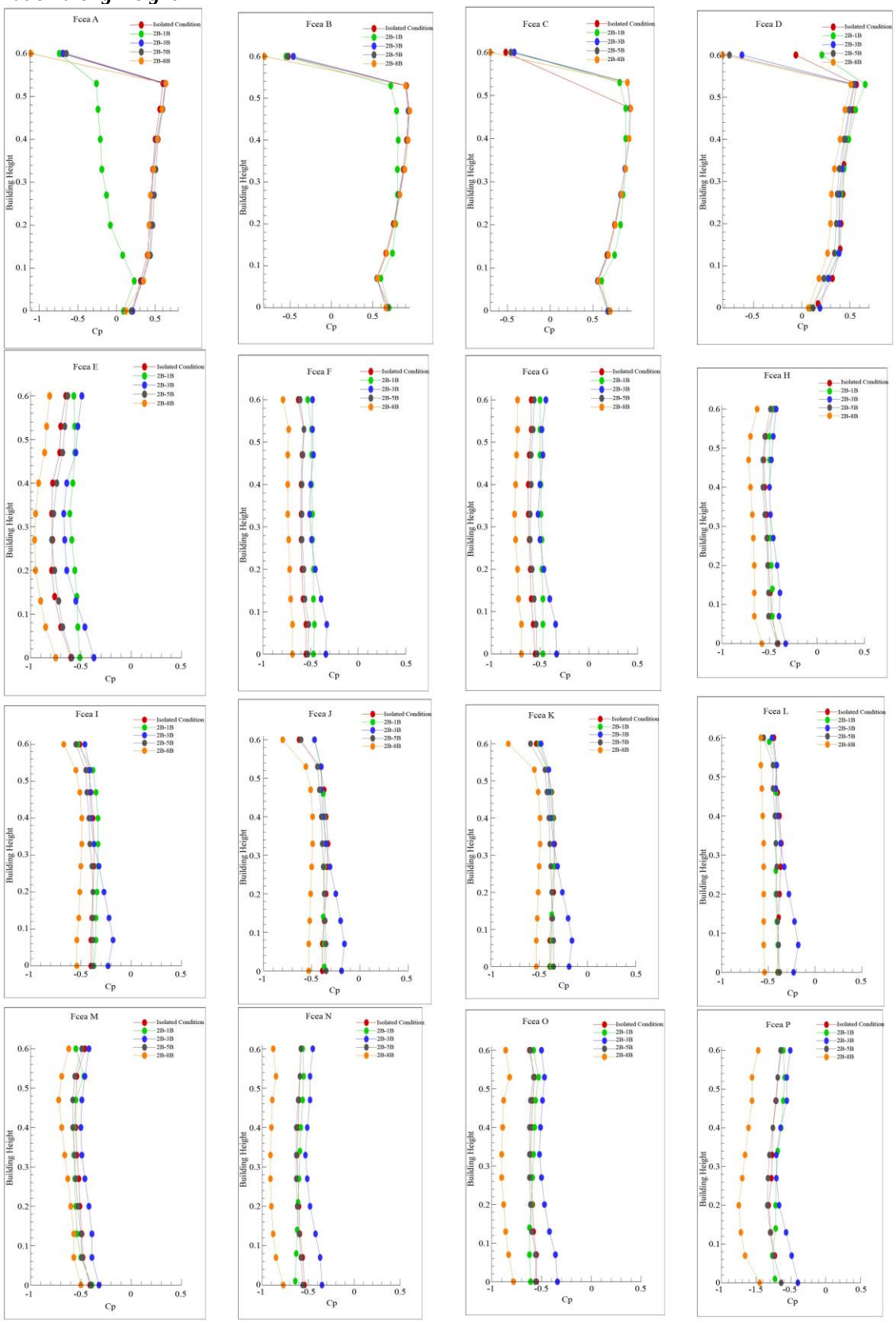

Fig. 16 Comparison of pressure coefficient along vertical centreline on each face of Case-1

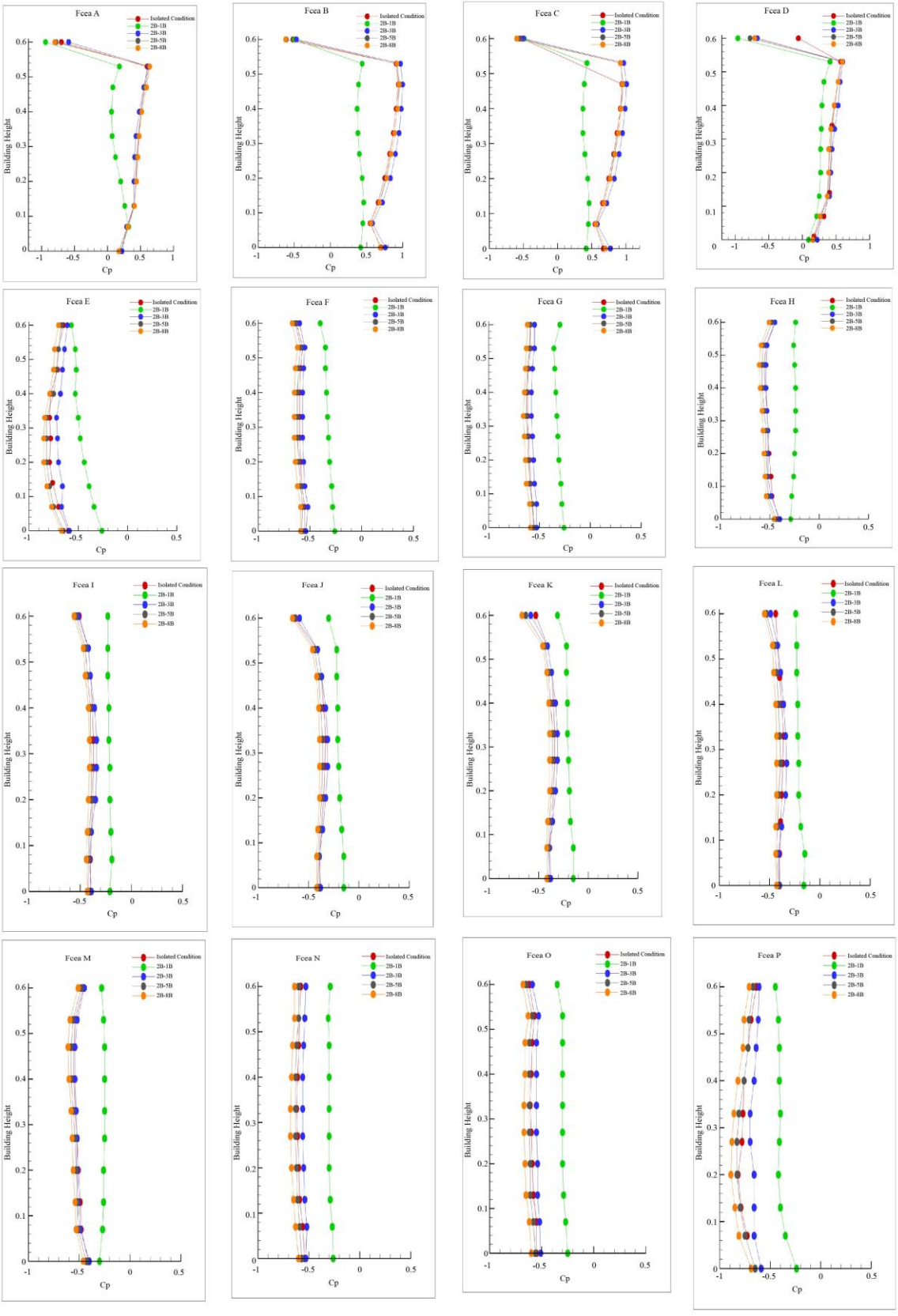

Fig. 17 Comparison of pressure coefficient along vertical centreline on each face of Case-2

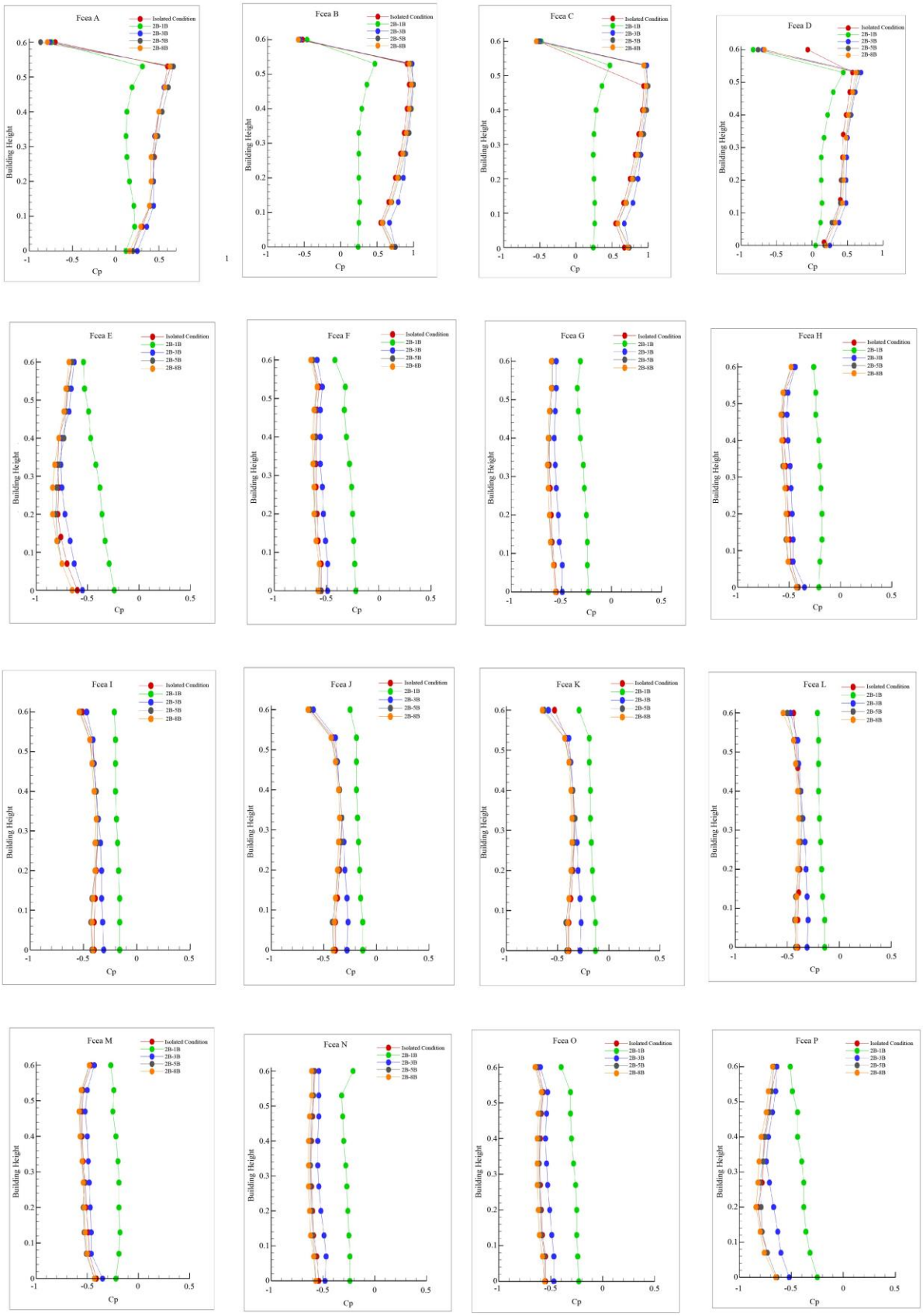

Fig. 18 Comparison of pressure coefficient along vertical centreline on each face of Case-3

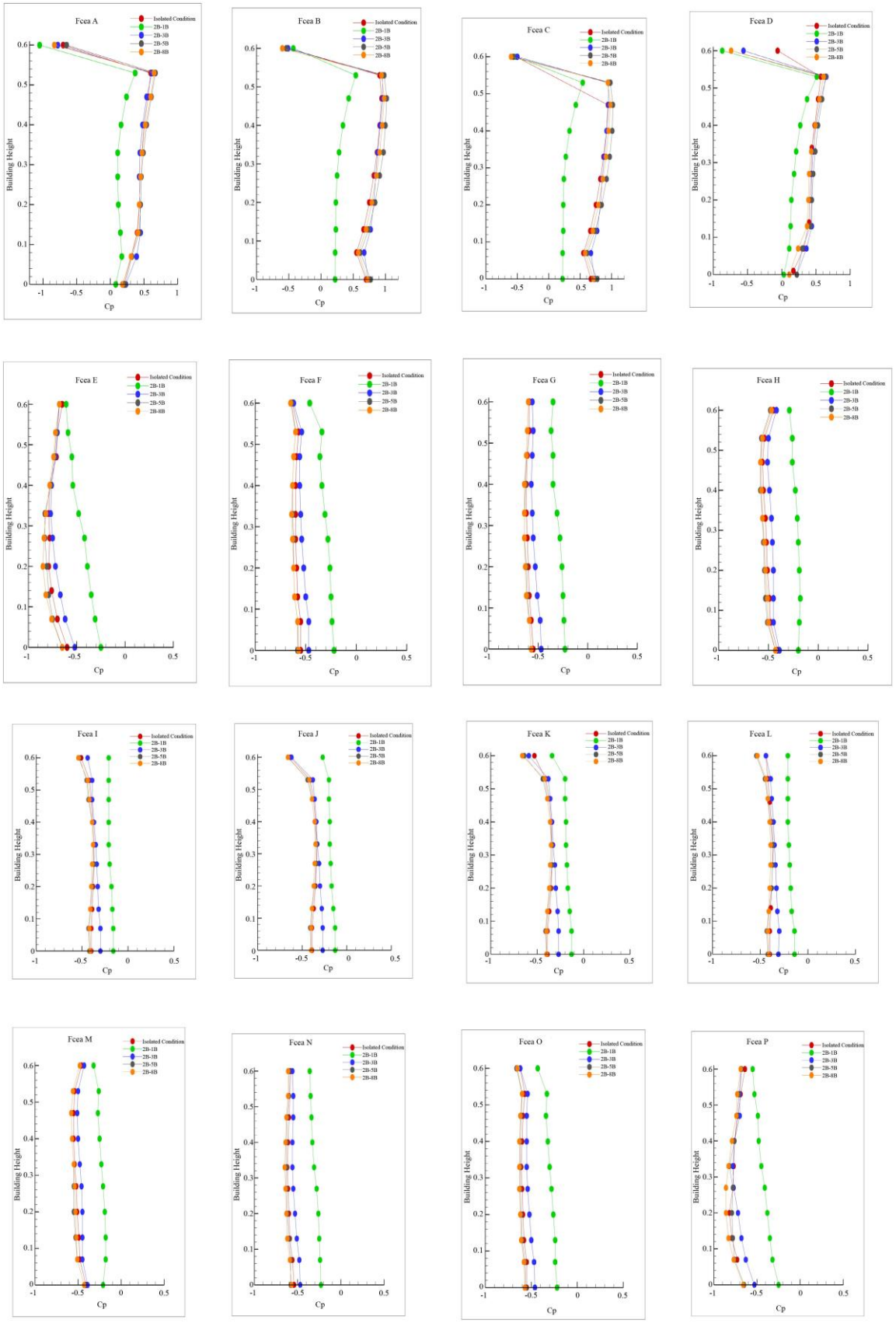

Fig. 19 Comparison of pressure coefficient along vertical centreline on each face of Case-4

The local pressure coefficients (Cp) on X-shaped building facades are influenced by building geometry and spacing [4, 23]. For the shortest spacing (Case I), the surrounding Y-shaped and octagonal buildings modify the approaching airflow, producing positive pressure coefficients (Cp) on the windward faces (B–C) and strong suction (−1.20) on the perimeter faces (M–P). The wake is compressed in the rectangular building in the downstream end, and the flow is redirected sideways in the Y-shaped building with an aerofoil shape, resulting in non-uniform pressure distribution and strong suction on the re-entrant surfaces (H-I). When spacing is increased (Cases II-III), localized building geometry impacts occur. There is not the same distribution of Cp around the Y-shaped structure, and less turbulent flow upstream than is seen in the octagonal shape. The wake is not compressible because it is rectangular in shape, and the wake re-joins very slowly but with a much higher rate of Cp recovery. Pressure distributions replicate those of the isolated configuration, in a wide range of configurations, under the maximum possible spacing in the longitudinal direction (Case IV: $S_1 = S = 10B$). At a distance of 1B ($S_k = 1B$), however, there is still significant shielding from the target, with interference factors between + 0.40 and + 0.95 in the windward direction, compared to those between − 0.30 and − 0.90 in the side and leeward direction. The aircraft response of an X-shaped building is affected by both the shape and distance between the buildings that are competing for the space, as these results show. The compact design will help create a smoother reattachment of the flow at a wider spacing between wing tips, but the Y-shaped interferer will generate more uniform suction flow at a narrow spacing between wing tips. They reduce the interference effects by increasing the distance along the buildings, whereas the distance laterally and the design of the neighbouring buildings are also important. Both contribute to reducing the aerodynamic stresses on buildings with complicated urban plans [7]. To find out how close-by buildings affect the surface pressure distribution of the X-shaped building, the four cases were compared by comparing the pressure coefficient distribution at the center line of the vertical direction for each face. The results are compared in the following figures: Case I, Case II, Case III, Case IV 16, 17, 18, and 19, respectively. These comparisons enable the detection of variations in pressure coefficients around the building faces under various interference situations, and help to understand how neighbouring building configurations affect the wind-induced pressure distribution.

4. Interference Factor (IF) Analysis

4.1. Definition and Calculation of Interference Factor

The effect of neighbouring buildings on the surface pressure characteristics of the principal X-shaped building was quantified using an Interference Factor (IF), defined as the ratio of the mean pressure coefficient under interference conditions to that under isolated conditions at the corresponding building face and height [28].

$$IF = \frac{C_{p,\,interference}}{C_{p,\,isolated}}$$

Where Cp,int and Cp,iso denote the mean pressure coefficients under interference and isolated conditions, respectively. The use of pressure-coefficient ratios provides a normalized measure for comparing the influence of neighbouring buildings under different spacing and building-face configurations [25, 28].

The pressure regime determines what kind of meaning the IF has since Cp is signed. In the case of positive pressure on the windward side, IF>1 indicates enhancement, and IF<1 indicates the amplitude of pressure is diminished compared to its amplitude under the conditions of no wind. The value of |Cp| is used to measure changes in the pressure below the level of the free stream (suction): Higher values of |Cp| mean greater suction. Although there may have been values near zero in the denominator, no adjustment was needed for this study because the values for the Cps in isolation were far enough from zero that performed the computation of IF were sufficient. The reported IF values were calculated straight from the interference and isolated Cp values in the same building with the same face and height. The interference Factors at Different Spacing configuration (Face-wise values A-P) shown in Table 4.

From the interference response point of view, the distance between the end of the longitudinal and end of the lateral axes is critical, as indicated by the statistical summary of the interference response. The mean IF is 0.812 when (S2) is 3B, and 1.197 when (S2) is 8B, illustrating that lateral separation does not decrease in uniform increments as (S2) increases. The largest face-wise IF is 1.46 at (S1=S3=2B) and (S2=8B). Instead, all faces stay below unity for (S1=S3=5B), (S2=1B), (8B), and (10B) with (1B). The larger the lateral spacing, the closer to unity the mean IF is for higher longitudinal separations. The results indicate that the spacing alone is not responsible for the interference response, and that both the face and the relative longitudinal and lateral positioning affect pressure response.

4.2. Face-wise Mean Interference Factor vs Spacing

The change of mean interference factor for Cases 1-4 with lateral spacing is shown as a face-wise variation in Figure 20. The results show that aerodynamic interference behaviour is highly dependent on spacing and face location of the X-shaped building. Strong interference effects are observed particularly on the upper-side, leeward, and perimeter faces (M–P) in Case 1 ($S_1 = S_3 = 2B$). Secondary wakes interaction and flow reattachment effects are observed with the increase of interference factor at larger lateral spacing. There is little variation in windward faces. When the spacing $S_1 = S_3 = 5B$ (Case 2), interference is less intense than in Case 1, but remains moderately intense on upper side and leeward faces at greater lateral spacing. This implies a continued influence

from lateral channelling and wake interaction. For Case 3 ($S_1 = S_3 = 8B$), interference effects are further reduced, and most of the face groups have values near to unity. This means more ability to recover from a wake and less aerodynamic interaction. For Case 4 ($S_1 = S_3 = 10B$), the interference response is reduced for many configurations, particularly at larger lateral spacings.

However, at $S_2 = 1B$, the face-wise IF values range from 0.23 to 0.56, indicating substantial shielding. Thus, the effect of increasing longitudinal spacing is not uniform and depends on the lateral spacing and the building face considered. The overall results indicate that the main effect of spacing in controlling aerodynamic interference is the effect of upper side and leeward faces.

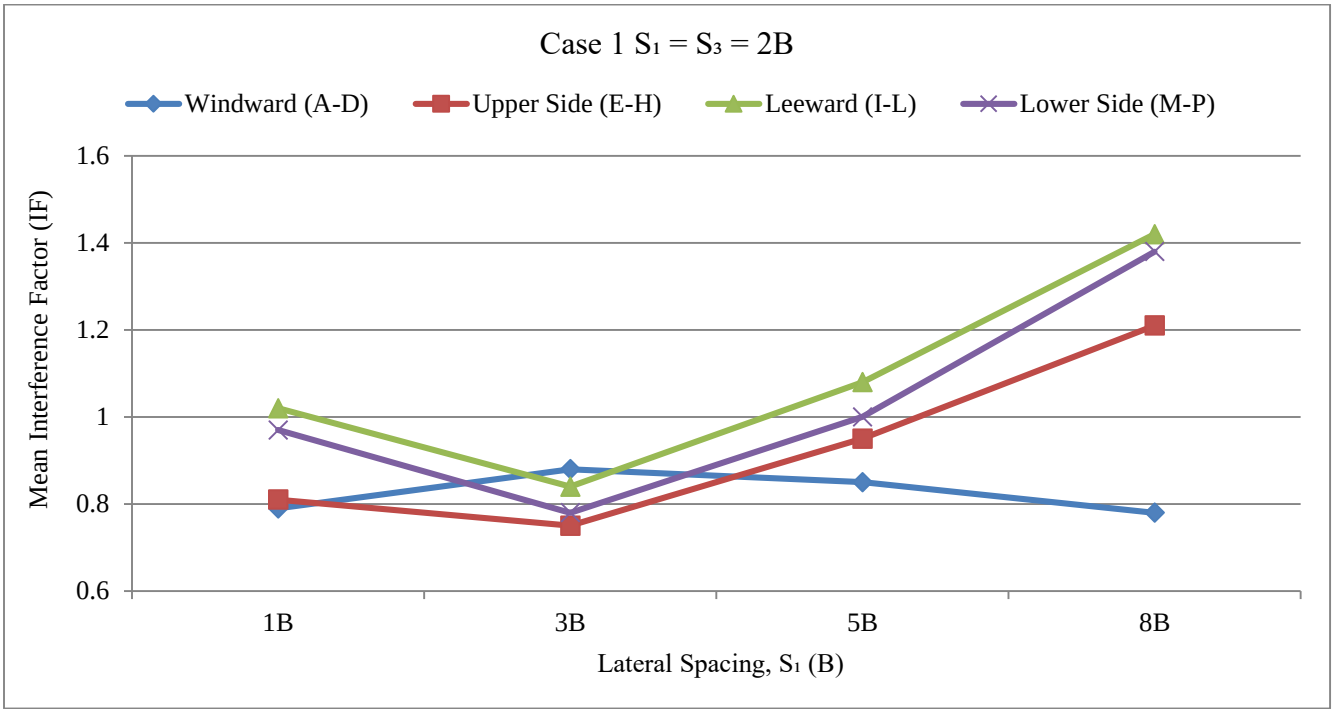

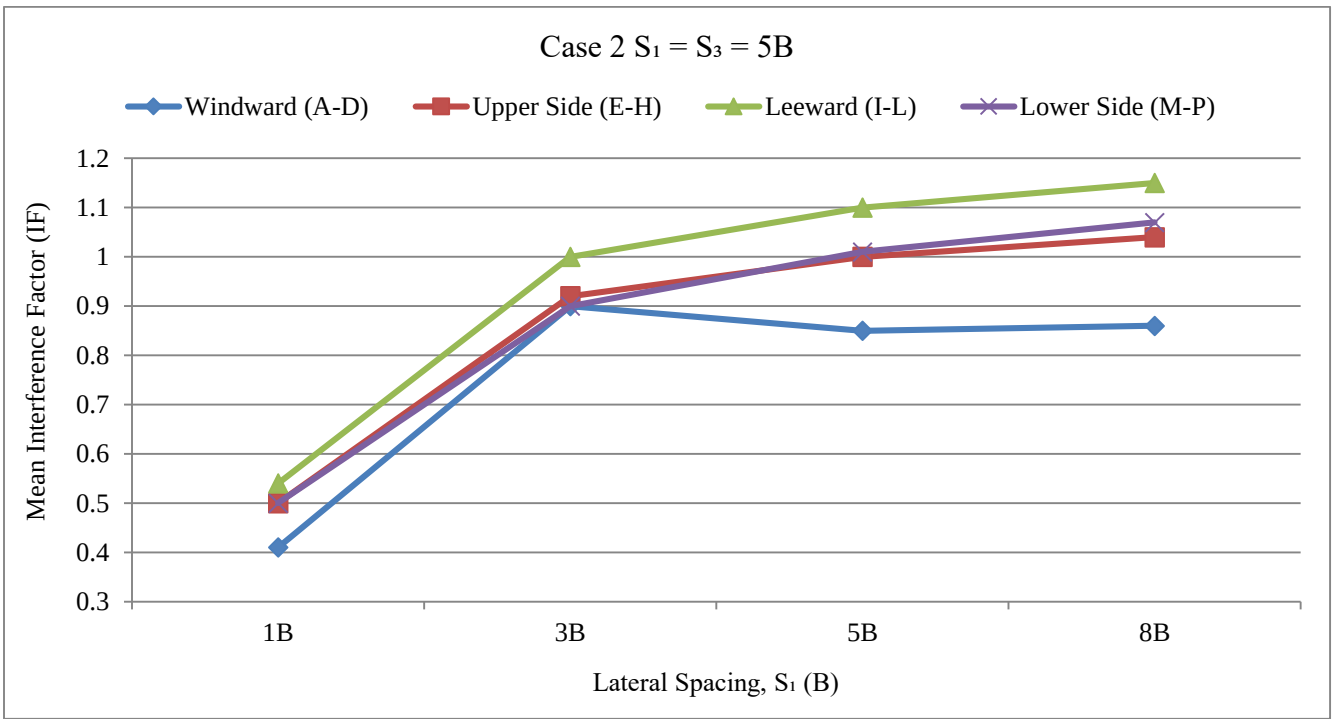

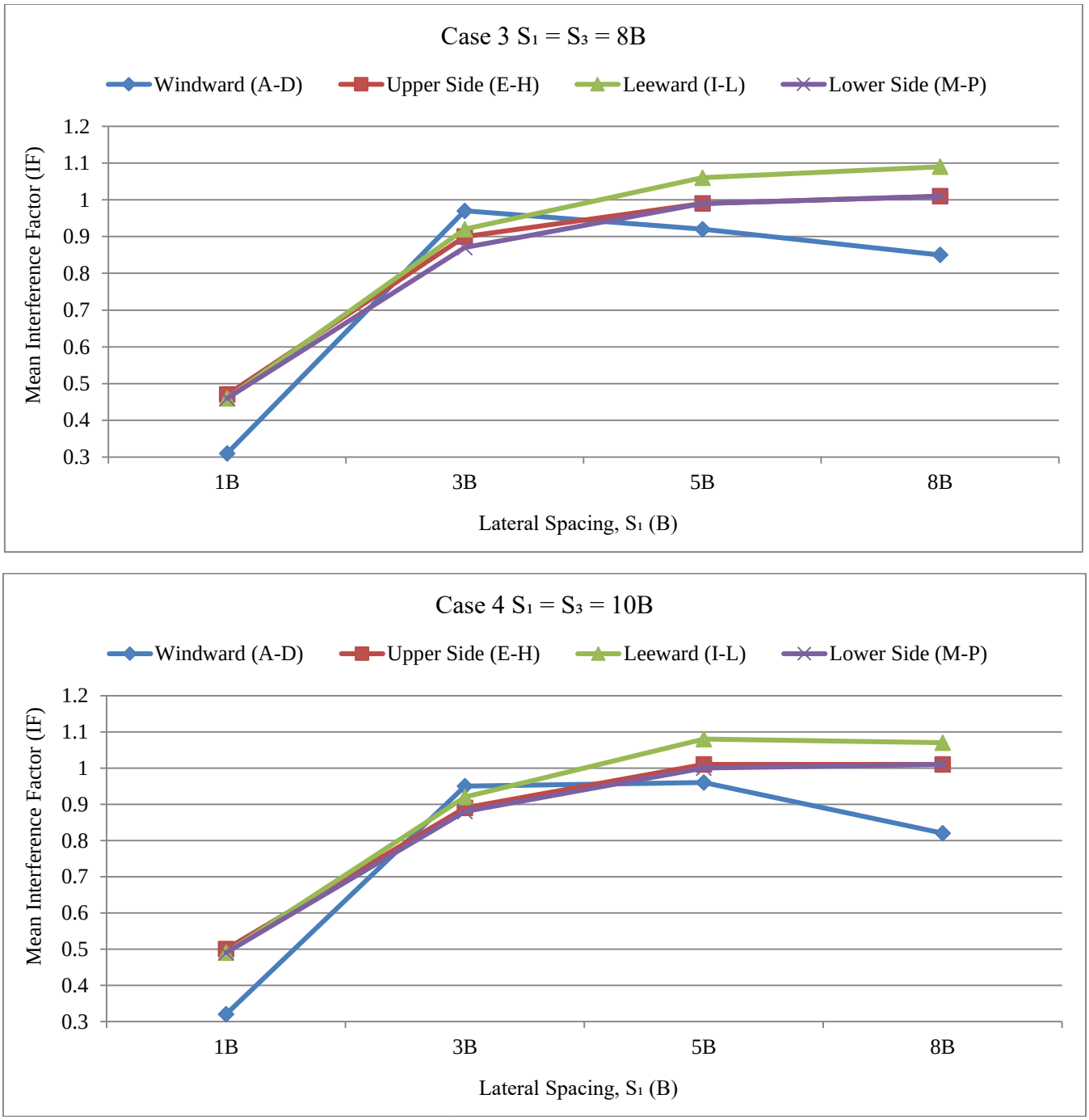

Fig. 20 Mean interference factor vs spacing for Case 1 – Case 4

4.3. Effect of Spacing on Interference Factor Distribution

Aerodynamic interference factors evolve as a function of both face and spacing. Along with the length of a building, separation has a diluting effect on the rest of the building, while separation along the sides can draw attention towards the face. It is shown that lateral separation does not always result in continuous attenuation [25] when the mean IF for S1=S3=2B varies from 0.812 at S2=3B to 1.197 at S2=8B. Although there is a good level of protection at S_2 = 1B, a number of designs have less interference response at $S_1 = S_3$ = 8B and 10B. Thus, if increased longitudinal length and width are beneficial to reduce interference, they do not guarantee that the IFs will be joined together on all the faces. Position of the face and distance between its sides determine the reaction.

This is due to the complex X-shaped geometry's shielding, flow channeling, wake interaction and local flow reattachment [25-28, 30].

4.4. Face-wise Amplification and Shielding Trends

For spacing configuration and face-wise positioning, aerodynamic response has been found to be affected by the interference factors of the face. For Windward faces (A-D), they either protect or enhance, depending on the specifications for long and lat spacing. Face A's IF is 0.31 at $S_1 = S_t = 2B$ and $S_k = 1B$, while Face D's is 1.11. Both sets of scores (E-H), show considerable variation in the upper. The IF values for Faces F, G, and H are 1.23, 1.22, and 1.28, respectively, at $S_1 = S_3 = 2B$ and $S_2 = 8B$, in comparison to the solo situation. In the case of $S_1 = S_t = 5B$, Face H has an IF of 1.02, while Faces J and K have IFs of 1.11 and 1.11, respectively. Although one might think it is possible to see a collectively selected answer in face, these figures emphasize the need to analyze individual expressions.

A leeward spacing design will have an effect on leeward face attenuation and amplification. Faces I-L IF values vary from 1.35 to 1.46 there is an appreciable amplification on S1 = S3 = 2B and on S2 = 8B. The shielding IF values for the faces at $S_1 = S_t = 10B$ and $S_k = 1B$ varied from 0.48 to 0.50. For all the configurations studied, the two (M-P) remaining perimeter faces also show configuration dependent response, with IF values, both above and below unity. M-P interference factors must not be considered as variations of the building elevations, it is a face-by-face assessment. Various factors, such as positioning of the faces, the lateral spacing, and the longitudinal spacing, all affect the shielding and amplification effect.

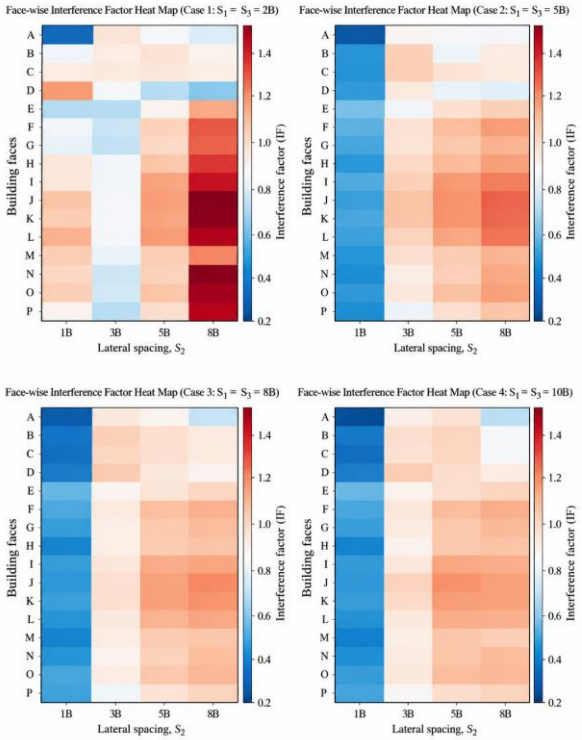

Fig. 21 Heat-map comparison of face-wise average Interference Factors (IF) for Cases 1–4 corresponding to increasing upstream and downstream spacing ($S_1 = S_3 = 2B–10B$)

Design-wise, it is recommended that, e.g. local pressure amplification and shielding be evaluated for all the relevant façade faces and spacing configurations, based on the face-wise results. Configurations with IF value much larger than 1 might provide more local suction or pressure than the isolated state; thus, other such cases need to be watched closely. Conclusions that one set of faces is more important than another, for any spacing, are dismissed by the results. Note: See Figure 21 for an average face-wise Interference Factors (IF) comparison (heat map) between the up and downstream spacing configuration with S1=S3=2B for Cases 1-4 for increasingly larger spacing: 2B to 10B. The further the distance from the main building to nearby buildings, the more the heat map visually changes, reflecting the change of interference factors that can be seen on average. This provides an easy means for us to compare and assess the interference effect for various alternative building faces and spacings.

5. Engineering Implications for Structural Design

This part presents the results of the interference analysis from more of a practical standpoint, with considerations for design of clustered tall buildings, code applicability and load estimate.

5.1. Interference Conditions Relevant to Structural Design

The results from interference measurements indicate that there is a possibility of pressure amplification in certain areas when longitudinal and lateral spacing are variable. The highest face-wise IF is 1.46 for S1=S3=2B, S2=8B, but other configurations yield IF values greater than one. The results demonstrate that localized interference varies with the spacing configuration and building-face location, indicating the need to evaluate multiple spacing arrangements. For local façade and structural pressure impacts, consider the building face impacted, longitudinal and lateral spacing.

5.2. Implications for Along-Wind Load Estimation

The aerodynamic response to 0° wind incidence is mostly regulated by along-wind loading (stagnation pressure on windward faces and suction on leeward and re-entrant surfaces). In situations I and II, the presence of the Y-shaped and octagonal structures upstream cause tight spacing, strong channeling jets and wake interference, increasing mean pressure differentials and drag forces on the X-shaped structure. The separated wake is further influenced by the downstream rectangular building, which modifies the wake structure and produces regions of high suction and substantial mean-pressure differences on the leeward façades. The spacing is increased (Cases III and IV), the flow field is even more stable, the wake length is reduced, and the suction intensity is reduced, resulting in pressure coefficients which are closer to isolated condition. The progressive attenuation means that the inter-building spacing ratio (S/H) is an important parameter to control the along-wind load

amplification. The results indicate that the pressure redistribution around an isolated building caused by other buildings may not be fully captured by pressure coefficients alone. Therefore, a CFD analysis or wind-tunnel analysis can be useful to examine pressure effects caused by the interference of clustered structures with complex plan geometry. For irregular planform and dense spacing, the load estimates along wind should be based on CFD or wind tunnel validation [16].

5.3. Limitations of Code-based Interference Provisions

IS 875 (Part 3): 2015 provides interference factors for the estimation of wind effects under specified building configurations [13]. Such code-based provisions are intended primarily for practical and preliminary assessment and may not explicitly represent the detailed face-wise pressure redistribution associated with complex non-convex building geometries. The present results indicate that the interference response of the X-shaped building varies with surrounding-building geometry, longitudinal spacing, lateral spacing, and affected building face. Therefore, the application of simplified code-based interference provisions to complex-plan tall buildings should be considered with appropriate caution. For such configurations, detailed CFD analysis or experimental investigation can provide additional information on localized pressure amplification, shielding, and wake interaction.

5.4. Design Relevance for Clustered Tall Buildings with Complex Shapes

The results demonstrate that the aerodynamic pressure sensitivity of the tall densely packed building with complex geometry is influenced by the geometry of the neighboring buildings in addition to the space between them. Although the total interference response is more or less close to the isolated state, localized pressure amplification and shielding can occur, as evidenced from the face-wise fluctuations of the interference factor response observed. The surrounding-building arrangement and spacing should thus be considered in the preliminary aerodynamic assessment of a complex plan tall structure. On the basis of the numerical basis the current results offer, configurations that need to be further examined, either through experimental testing in the wind tunnel or through CFD refinement, can be pinpointed.

6. Limitations of the Study

These limitations are intrinsic to the study's scope and do not invalidate the observed mean pressure trends and interference mechanisms.

6.1. Rigid Building Assumption

The present CFD analysis was executed on the basis of rigid, non-deformable building surfaces, and without considering possible aeroelastic interaction between wind-induced loads and structural motion. This technique can be applied to determine the mean pressure pattern and interference of the flow, but cannot be used to record dynamic feedback effects such as load redistribution due to motion or resonance under variable wind loads. Under real-world conditions, flexible tall buildings may have load amplification or damping that is not covered by the simplified approach. These coupled effects should be quantifiable in the future using Fluid–Structure Interaction (FSI) or aeroelastic wind tunnel testing [33].

6.2. Single Wind Direction or Limited Angles

The simulations were conducted at a wind incidence angle of 0°, and the results characterize the aerodynamic response for this specific wind direction. Further simulations at additional wind incidence angles are required to determine whether other directions produce more critical aerodynamic responses. But in reality, urban conditions involve multi-directional wind exposure and oblique angles of wind (30°, 45°) will greatly affect flow separation, wake deflection and local suction. Aerodynamic interference patterns seen at 0° may not be representative of the patterns seen at other approach angles. The 0° wind incidence angle provides a reference for evaluating the mean pressure distribution and interference effects under the investigated spacing configurations. Additional wind incidence angles are required to determine whether other directions produce more critical aerodynamic responses.

6.3. Absence of Aeroelastic and Transient Effects

The present study deals with steady state Reynolds-Averaged Navier–Stokes (RANS) simulation that is able to capture the mean flow and mean pressure characteristics, but will underpredict unsteady vortex shedding and transient load peaks. Thus, the present analysis is dedicated to mean aerodynamic behavior, while peak transient loads and fatigue effects are noted as important items for future study. Large Eddy Simulation (LES) or unsteady hybrid turbulence models may be used to improve the prediction of wake dynamics and peak pressure estimation, providing more insight into structural response prediction in real turbulence conditions.

7. Conclusion

The changes in the aerodynamic performance of X-shaped tall building were systematically analyzed by a two-dimensional Computational Fluid Dynamics (CFD) model in both isolated and interference wind attack cases with the wind approaching at an angle of attack of 0°. Computational Fluid Dynamics (CFD) models and the traditional k-ε turbulence model were used to analyze the wind attack effect on the aerodynamic performance of the X-shaped tall building, both isolated and interference cases. The separated flow from the corners, the stalling flow on the windward surfaces, and the reattachment region downstream from the building were all observed in the present CFD results of the isolated-building study. The interference analysis demonstrated that neighbouring buildings significantly modify the surface-pressure distribution of the X-shaped building through flow channelling, shielding, wake interaction, and local flow

reattachment. The magnitude and direction of the interference response depended on longitudinal spacing, lateral spacing, surrounding-building configuration, and building-face location. Increasing longitudinal separation generally reduced the overall influence of neighbouring buildings; however, the extent of this reduction depended on lateral spacing and building-face location. At $S_1 = S_3 = 10B$ (S/H = 2.50), substantial shielding persisted at $S_2 = 1B$, where the face-wise interference factors ranged from 0.23 to 0.56. Therefore, the 10B configuration did not uniformly reproduce the isolated-building condition. These findings demonstrate the importance of considering surrounding-building geometry and spacing when assessing wind-induced pressures on complex-plan tall buildings. The present study is limited to a wind incidence angle of 0° and steady-state CFD simulations. Further investigations should consider additional wind directions, unsteady flow effects, aeroelastic/FSI analyses, and experimental validation to extend the applicability of the findings to more complex urban configurations.

References

[1] Yangluxi Li, and Lei Chen, "Study on the Influence of Voids on High-Rise Building on the Wind Environment," *Building Simulation*, vol. 13, no. 2, pp. 419-438, 2020. [CrossRef] [Google Scholar] [Publisher Link]

[2] Jiachen Lu et al., "Representing the Effects of Building Height Variability on Urban Canopy Flow," *Quarterly Journal of the Royal Meteorological Society*, vol. 150, no. 758, pp. 46-67, 2024. [CrossRef] [Google Scholar] [Publisher Link]

[3] Arghyadip Das, Rajdip Paul, and Sujit Kumar Dalui, "Shape Optimization of Corner Recessed Square Tall Building Employing Surrogate Modelling," *Wind and Structures*, vol. 36, no. 2, pp. 105-120, 2023. [CrossRef] [Google Scholar] [Publisher Link]

[4] Debasish Kumar, and Sujit Kumar Dalui, "Effect of Internal Angles Between Limbs of Cross Plan Shaped Tall Building Under Wind Load," *Wind and Structures*, vol. 24, no. 2, pp. 95-118, 2017. [CrossRef] [Google Scholar] [Publisher Link]

[5] S. Thepmongkorn, G.S Wood, and K.C.S Kwok, "Interference Effects on Wind-Induced Coupled Motion of Tall Buildings," *Journal of Wind Engineering and Industrial Aerodynamics*, vol. 90, no. 12-15, pp. 1807-1815, 2002. [CrossRef] [Google Scholar] [Publisher Link]

[6] U.F. Tang, and K.C.S. Kwok, "Interference Excitation Mechanisms on a 3DOF Aeroelastic CAARC Building Model," *Journal of Wind Engineering and Industrial Aerodynamics*, vol. 92, nos. 14-15, pp. 1299-1314, 2004. [CrossRef] [Google Scholar] [Publisher Link]

[7] Himanshoo Verma, and R. S. Sonparote, "Numerical Investigation of Wind Interference Effect on Twin C-Shaped Tall Buildings," *Wind and Structures*, vol. 37, no. 6, pp. 425-444, 2023. [CrossRef] [Google Scholar] [Publisher Link]

[8] Suresh K Nagar, Ritu Raj, and Nirendra Dev, "Experimental Study of Wind-Induced Pressures on Tall Buildings of Different Shapes," *Wind and Structures*, vol. 31, no. 5, pp. 431-443, 2020. [CrossRef] [Google Scholar] [Publisher Link]

[9] J.G. Zhao, and K. M. Lam, "Interference Effects in Groups of Tall Buildings Arranged in L- and T-Shaped Patterns," *Wind and Structures*, vol. 11, no. 1, pp. 1-18, 2008. [CrossRef] [Google Scholar] [Publisher Link]

[10] N. Agarwal, A.K. Mittal, and V.K. Gupta, "Along-Wind Interference Effects on Tall Buildings," *Proceedings of the 6th National Conference on Wind Engineering*, India, pp. 193-204, 2012. [Google Scholar]

[11] Hideyuki Tanaka et al., "Experimental Investigation of Aerodynamic Forces and Wind Pressures Acting on Tall Buildings with Various Unconventional Configurations," *Journal of Wind Engineering and Industrial Aerodynamics*, vol. 107-108, pp. 179-191, 2012. [CrossRef] [Google Scholar] [Publisher Link]

[12] ASCE/SEI 7-10, *Minimum Design Loads for Buildings and Other Structures*, American Society of Civil Engineers, 2010. [Google Scholar] [Publisher Link]

[13] Bureau of Indian Standards, "*IS: 875(Part3): Wind Loads on Buildings and Structures -Proposed Draft & Commentary*, pp. 1-105, 2015. [Google Scholar] [Publisher Link]

[14] *AS/NZS 1170.2: Structural design actions, Part 2: Wind Actions*, Standards Australia, 2011. [Publisher Link]

[15] A.C. Khanduri, T. Stathopoulos, and C. Bédard, "Wind-Induced Interference Effects on Buildings - A Review of the State-of-the-art," *Engineering Structures*, vol. 20, no. 7, pp. 617-630, 1998. [CrossRef] [Google Scholar] [Publisher Link]

[16] Min Kyu Kim, Soonpil Kang, and Thomas H.-K. Kang, "Practical Applications of Computational Fluid Dynamics to Wind Design of High-Rise Buildings," *Wind and Structures*, vol. 39, no. 4, pp. 287-304, 2024. [CrossRef] [Google Scholar] [Publisher Link]

[17] Prasenjit Sanyal, and Sujit Kumar Dalui, "Comparison of Aerodynamic Coefficients of Various Types of Y-Plan-Shaped Tall Buildings," Asian Journal of Civil Engineering, vol. 21, no. 7, pp. 1109-1127, 2020. [CrossRef] [Google Scholar] [Publisher Link]

[18] Ben Mou et al., "Numerical Simulation of the Effects of Building Dimensional Variation on Wind Pressure Distribution," *Engineering Applications of Computational Fluid Mechanics*, vol. 11, no. 1, pp. 293-309, 2017. [CrossRef] [Google Scholar] [Publisher Link]

[19] Giancarlo Alfonsi, "Reynolds-Averaged Navier–Stokes Equations for Turbulence Modeling," *Applied Mechanics Reviews*, vol. 62, no. 4, pp. 1-20, 2009. [CrossRef] [Google Scholar] [Publisher Link]

[20] Nidhal Hnaien et al., "CFD Analysis of Wind Distribution around Buildings in Low-Density Urban Community," *Mathematics*, vol. 10, no. 7, pp. 1-14, 2022. [CrossRef] [Google Scholar] [Publisher Link]

[21] Jörg Franke et al., "Recommendations on the Use of CFD in Wind Engineering," *COST Action C14*, pp. 529-532, 2004. [Google Scholar] [Publisher Link]

[22] Bert Blocken, Ted Stathopoulos, and Jan Carmeliet, "CFD Simulation of the Atmospheric Boundary Layer: Wall Function Problems," *Atmospheric Environment*, vol. 41, no. 2, pp. 238-252, 2007. [CrossRef] [Google Scholar] [Publisher Link]

[23] Rajdip Paul, and Sujit Kumar Dalui, "Wind Effects on Z Plan-Shaped Tall Building," *International Journal of Advanced Structural Engineering*, vol. 8, no. 3, pp. 319-335, 2016. [CrossRef] [Google Scholar] [Publisher Link]

[24] B.E. Lee, and B. F. Soliman, "An Investigation of the Forces on Three Dimensional Bluff Bodies in Rough Wall Turbulent Boundary Layers," *Journal of Fluids Engineering*, vol. 99, no. 3, pp. 503-509, 1977. [CrossRef] [Google Scholar] [Publisher Link]

[25] Wonsul Kim, Yukio Tamura, and Akihito Yoshida, "Interference Effects on Aerodynamic Wind Forces between Two Buildings," *Journal of Wind Engineering and Industrial Aerodynamics*, vol. 147, pp. 186-201, 2015. [CrossRef] [Google Scholar] [Publisher Link]

[26] Hiromasa Nakayama, Tetsuya Takemi, and Haruyasu Nagai, "LES Analysis of the Aerodynamic Surface Properties for Turbulent Flows over Building Arrays with Various Geometries," *Journal of Applied Meteorology and Climatology*, vol. 50, no. 8, pp. 1692-1712, 2011. [CrossRef] [Google Scholar] [Publisher Link]

[27] Md Mahbub Alam, Y. Zhou, and X.W. Wang, "The Wake of Two Side-by-side Square Cylinders," *Journal of Fluid Mechanics*, vol. 669, pp. 432-471, 2011. [CrossRef] [Google Scholar] [Publisher Link]

[28] Rony Kar, and Sujit Kumar Dalui, "Wind Interference Effect on an Octagonal Plan-Shaped Tall Building due to Square Plan-Shaped Tall Buildings," *International Journal of Advanced Structural Engineering*, vol. 8, no. 1, pp. 73-86, 2016. [CrossRef] [Google Scholar] [Publisher Link]

[29] Yasuyuki Ishida et al., "Impact of a Single High-Rise Building on the Wind Pressure Acting on the Surrounding Low-Rise Buildings," *Journal of Wind Engineering and Industrial Aerodynamics*, vol. 250, pp. 1-13, 2024. [CrossRef] [Google Scholar] [Publisher Link]

[30] Bharat Singh Chauhan, Anupam Chakrabarti, and Ashok Kumar Ahuja, "Study of Wind Loads on Rectangular Plan Tall Building under Interference Condition," *Structures*, vol. 43, pp. 105-130, 2022. [CrossRef] [Google Scholar] [Publisher Link]

[31] Kasun Wijesooriya et al., "A Technical Review of Computational Fluid Dynamics (CFD) Applications on Wind Design of Tall Buildings and Structures: Past, Present and Future," *Journal of Building Engineering*, vol. 74, pp. 1-24, 2023. [CrossRef] [Google Scholar] [Publisher Link]

[32] Pradeep K. Goyal et al., "Numerical Study of Wind Loads on Y Plan-Shaped Tall Building Using CFD," *Civil Engineering Journal*, vol. 8, no. 2, pp. 263-277, 2022. [CrossRef] [Google Scholar] [Publisher Link]

[33] U.F. Tang, and K.C.S. Kwok, "Interference Excitation Mechanisms on a 3-DOF Aeroelastic CAARC Building Model," *Journal of Wind Engineering and Industrial Aerodynamics*, vol. 92, no. 14-15, pp. 1299-1314, 2004. [CrossRef] [Google Scholar] [Publisher Link]

[34] W.H. Melbourne, "Comparison of Measurements on the CAARC Standard Tall Building Model in Simulated Model Wind Flows," *Journal of Wind Engineering and Industrial Aerodynamics*, vol. 6, no. 1-2, pp. 73-88, 1980. [CrossRef] [Google Scholar] [Publisher Link]

Appendix

Table 4. Interference factors at different spacing configurations (Face-wise values A–P)

S3 (mm)	S1 (mm)	S2 (mm)	A	B	C	D	E	F	G	H	I	J	K	L	M	N	O	P
2B	2B	1B	0.31	0.84	0.89	1.11	0.7	0.82	0.81	0.92	0.92	1.04	1.03	1.07	1.01	0.99	1.0	0.86
		3B	0.9	0.89	0.89	0.84	0.7	0.75	0.74	0.83	0.83	0.84	0.84	0.84	0.83	0.77	0.77	0.73
		5B	0.86	0.9	0.89	0.73	0.87	0.97	0.96	1.0	1.06	1.09	1.08	1.09	1.01	1.01	1.02	0.94
		8B	0.79	0.87	0.88	0.59	1.1	1.23	1.22	1.28	1.35	1.46	1.45	1.42	1.21	1.46	1.45	1.39
5B	5B	1B	0.26	0.46	0.46	0.47	0.57	0.55	0.53	0.5	0.55	0.54	0.55	0.53	0.51	0.49	0.5	0.49
		3B	0.86	0.97	0.97	0.89	0.83	0.94	0.93	0.97	0.99	1.01	1.01	0.98	0.96	0.91	0.92	0.82
		5B	0.84	0.83	0.91	0.82	0.93	1.02	1.01	1.02	1.08	1.11	1.11	1.08	1.02	1.02	1.03	0.95
		8B	0.84	0.9	0.9	0.81	0.97	1.07	1.05	1.07	1.13	1.17	1.16	1.15	1.07	1.09	1.1	1.01
8B	8B	1B	0.3	0.33	0.31	0.32	0.51	0.49	0.47	0.41	0.47	0.46	0.47	0.46	0.42	0.45	0.48	0.5
		3B	0.91	0.99	0.98	1.0	0.86	0.91	0.9	0.9	0.92	0.93	0.93	0.9	0.89	0.87	0.89	0.83
		5B	0.87	0.95	0.95	0.91	0.92	1.02	1.01	1.01	1.06	1.08	1.08	1.05	1.01	1.0	1.01	0.92
		8B	0.7	0.92	0.91	0.88	0.95	1.03	1.02	1.01	1.07	1.12	1.1	1.07	1.01	1.03	1.04	0.96
10B	10B	1B	0.23	0.34	0.33	0.38	0.56	0.52	0.51	0.43	0.49	0.49	0.5	0.48	0.45	0.48	0.5	0.52
		3B	0.89	0.96	0.95	0.99	0.87	0.9	0.89	0.88	0.9	0.95	0.92	0.89	0.88	0.89	0.9	0.87
		5B	0.92	0.98	0.98	0.96	0.94	1.03	1.02	1.02	1.06	1.11	1.09	1.06	1.02	1.02	1.04	0.94
		8B	0.69	0.85	0.85	0.89	0.95	1.04	1.03	1.01	1.06	1.09	1.09	1.06	1.01	1.03	1.04	0.97